SCUOLA NORMALE SUPERIORE

INGV

Volcanic hazard assessement at Campi Flegrei caldera with uncertainty quantification

Andrea Bevilacqua
Istituto Nazionale di Geofisica e Vulcanologia, Sezione di Pisa
Scuola Normale Superiore di Pisa

Research study reported in the PhD thesis:
Doubly stochastic models for volcanic vent opening probability and pyroclastic density current hazard at Campi Flegrei caldera, Scuola Normale Superiore di Pisa, 2015.
Supervisors: Prof. Franco Flandoli, Dr. Augusto Neri.
Accepted for the publication in the series "PhD Thesis", Edizioni della Normale, Birkhäuser/Springer.

MEDiterranean SUpersite Volcanoes
MED-SUV

Istituto Nazionale di Geofisica e Vulcanologia, Sezione di Pisa
28th January 2016

The volcanological problem

Campi Flegrei is an active volcanic area in the Campanian Plain, dominated by a 12 km large caldera.

A few hundreds of thousand people live inside the caldera, and more than **1 million people** live in the nearby city of Naples.

The study concerns Campi Flegrei **long-term hazard assessments**, primarily based on past eruption data and on the structural features of the volcanic system.

They are required for **land use and evacuation planning**, but constitute also the necessary background for short-term hazard assessments.

Estimating the **probability of the next eruption event, its size, location, time and type** is a very difficult issue because of

- the lack of detailed information on the deeper portions of the system
- the high complexity of the physical processes controlling it.

Fig 2. Mosaic of orthophotos of Campi Flegrei caldera and surrounding areas

• Campi Flegrei caldera was created by **two ancient huge eruptions:** Campanian Ignimbrite (CI - 40 ka BP) and Neapolitan Yellow Tuff (NYT - 15 ka BP);

• In the last 15 ka the **eruption vents were sparse** in the caldera and most of the eruptions were explosive;

• There were **3 eruptive epochs** of volcanic activity, alternated to long periods of quiescence.

	Start	Duration
Epoch I	[15 ka BP	~4.5 ka]
Epoch II	[9.6 ka BP	~0.5 ka]
Epoch III	[5.5 ka BP	~2 ka]

•The most recent 'Monte Nuovo' eruption was in AD 1538, after ~3-3.5 ka of quiescience.

• Now there is much hydrothermal activity and the caldera is in an **unrest state**.

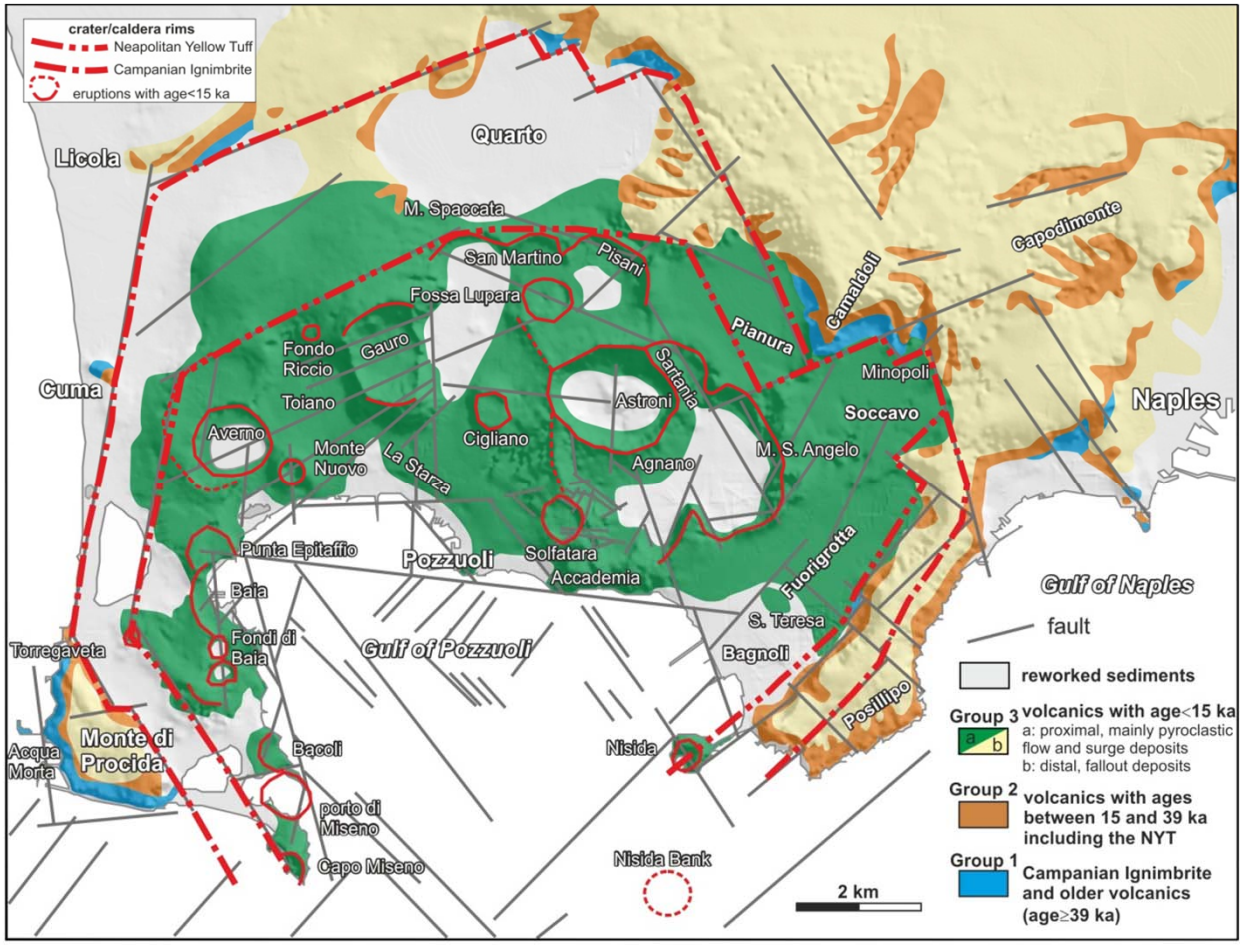

Fig 3. Simplified geological map of Campi Flegrei caldera showing regional fault traces and main morphological structures.

Methodology

The volcano is assumed as a **random system** that must be assessed with incomplete and **uncertain information**.

Adopting a **doubly stochastic approach,** the ill-constrained parameters of the probability models are themselves represented as additional random variables.

Uncertainty quantification assumes a great importance, and we distinguished:

I. the **physical variability,** i.e. the intrinsic randomness of the system under study,
II. the **epistemic uncertainty** due to the imperfect knowledge of the system.

As a consequence of this approach, all the probability estimates have their own confidence intervals.

Example: define X as the random result of an unknown dice, which could have 6 or 20 faces with equal chances.

The probability P of the event {X>3} is 50% in the first case, but it is 85% in the second.

Following a doubly stochastic approach, we will say that
P is 67.5% in mean, with an uncertainty range from 50% to 85%.

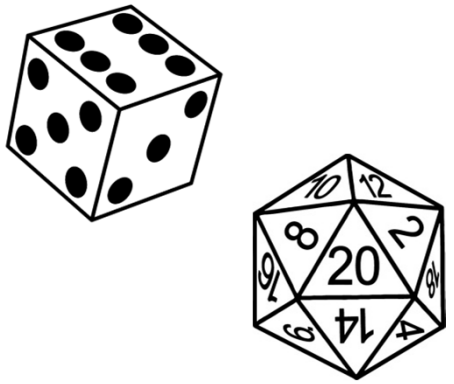

Even the probability maps will be affected by uncertainty: for this reason we calculated the **mean, 5th and 95th percentile** values for all the probability density functions and volcanic hazard estimates.

Outline

This study includes three main parts, dedicated to long term hazard probability assessments with a particular attention to the **uncertainty quantification**.

I. a map of probability for **the location** of the next eruptive vent
(see Bevilacqua et. al 2015)

II. a probability distribution for **the size** of the next pyroclastic density current (PDC), and a map of probability for the **PDC invasion hazard**
(see Neri et al. 2015)

III. a time-space probability model for **the time** of the next eruption, focused on the vents clustering

PART I

Vent opening probability maps

A key aspect of the study was the **identification**, and where possible the **quantification**, of some of the main **sources of epistemic uncertainty** that are associated with the available data.

• the **uncertainty on location** of past eruptive vents;

• the number of past events which do not correspond to presently identified locations ('**lost vents**');

• the **uncertainty of linear weights** of different probability measures contributing to the vent opening map definition.

The physical variability is assessed with a **linear combination** of 7 spatial distributions $(\mu_i)_{i=1,\dots,d}$ of key variables of the system that reflect, or can influence, this volcanic process.

Vents Epoch I	*Vents Epoch II*	*Vents Epoch III*	*Lost vents*	*Faults*	*Fractures*	*Homog. map*

It was included a uniform probability measure, **homogeneous** over the NYT caldera, for representing the possible lack of information. Lost vents have been assumed uniformly on the **inland** portion of the caldera.

The assessment of the vent opening map $\sum_{i=1}^{d} \alpha_i(e)\mu_i$, is reduced to find the distribution of the positive random coefficients $\alpha = (\alpha_i)_{i=1,\dots,d}$, $\sum_i^d \alpha_i = 1$ depending on the epistemic uncertainty *e*.

The first three probability maps are obtained from the renormalized sum of **uniform probability distributions** inside ellipses enclosing the **uncertain/enlarged locations** of past vents/fissures during each epoch of activity.

Large ellipses mostly indicate lack of constraints and **large uncertainty** in the locality of the vent.

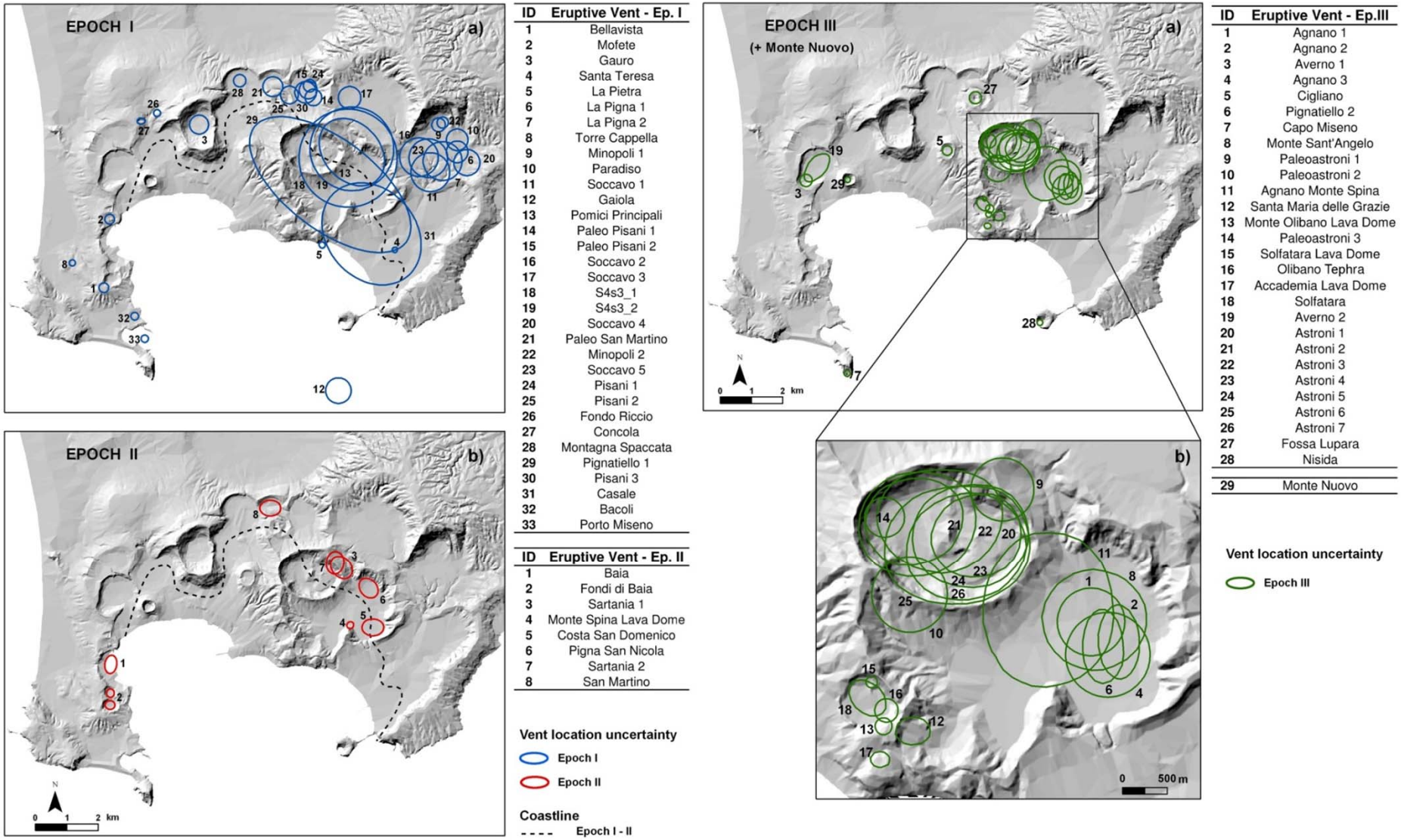

ID	Eruptive Vent - Ep. I
1	Bellavista
2	Mofete
3	Gauro
4	Santa Teresa
5	La Pietra
6	La Pigna 1
7	La Pigna 2
8	Torre Cappella
9	Minopoli 1
10	Paradiso
11	Soccavo 1
12	Gaiola
13	Pomici Principali
14	Paleo Pisani 1
15	Paleo Pisani 2
16	Soccavo 2
17	Soccavo 3
18	S4s3_1
19	S4s3_2
20	Soccavo 4
21	Paleo San Martino
22	Minopoli 2
23	Soccavo 5
24	Pisani 1
25	Pisani 2
26	Fondo Riccio
27	Concola
28	Montagna Spaccata
29	Pignatiello 1
30	Pisani 3
31	Casale
32	Bacoli
33	Porto Miseno

ID	Eruptive Vent - Ep. II
1	Baia
2	Fondi di Baia
3	Sartania 1
4	Monte Spina Lava Dome
5	Costa San Domenico
6	Pigna San Nicola
7	Sartania 2
8	San Martino

ID	Eruptive Vent - Ep.III
1	Agnano 1
2	Agnano 2
3	Averno 1
4	Agnano 3
5	Cigliano
6	Pignatiello 2
7	Capo Miseno
8	Monte Sant'Angelo
9	Paleoastroni 1
10	Paleoastroni 2
11	Agnano Monte Spina
12	Santa Maria delle Grazie
13	Monte Olibano Lava Dome
14	Paleoastroni 3
15	Solfatara Lava Dome
16	Olibano Tephra
17	Accademia Lava Dome
18	Solfatara
19	Averno 2
20	Astroni 1
21	Astroni 2
22	Astroni 3
23	Astroni 4
24	Astroni 5
25	Astroni 6
26	Astroni 7
27	Fossa Lupara
28	Nisida
29	Monte Nuovo

Fig 7. Reconstruction of the location of the eruptive vents and fissures for the events occurred in the three epochs of activity. The dashed line indicates the likely location of the coast line between Epochs II and III. Names of the events updated from Smith et al. 2011.

Based on experts opinion, we partitioned the caldera in 16 zones $(A_l)_{l=1,\dots,N}$ with different features and history of activity, separating the **spatial and temporal clusters** of past vents.
The first 13 zones have the same extent.

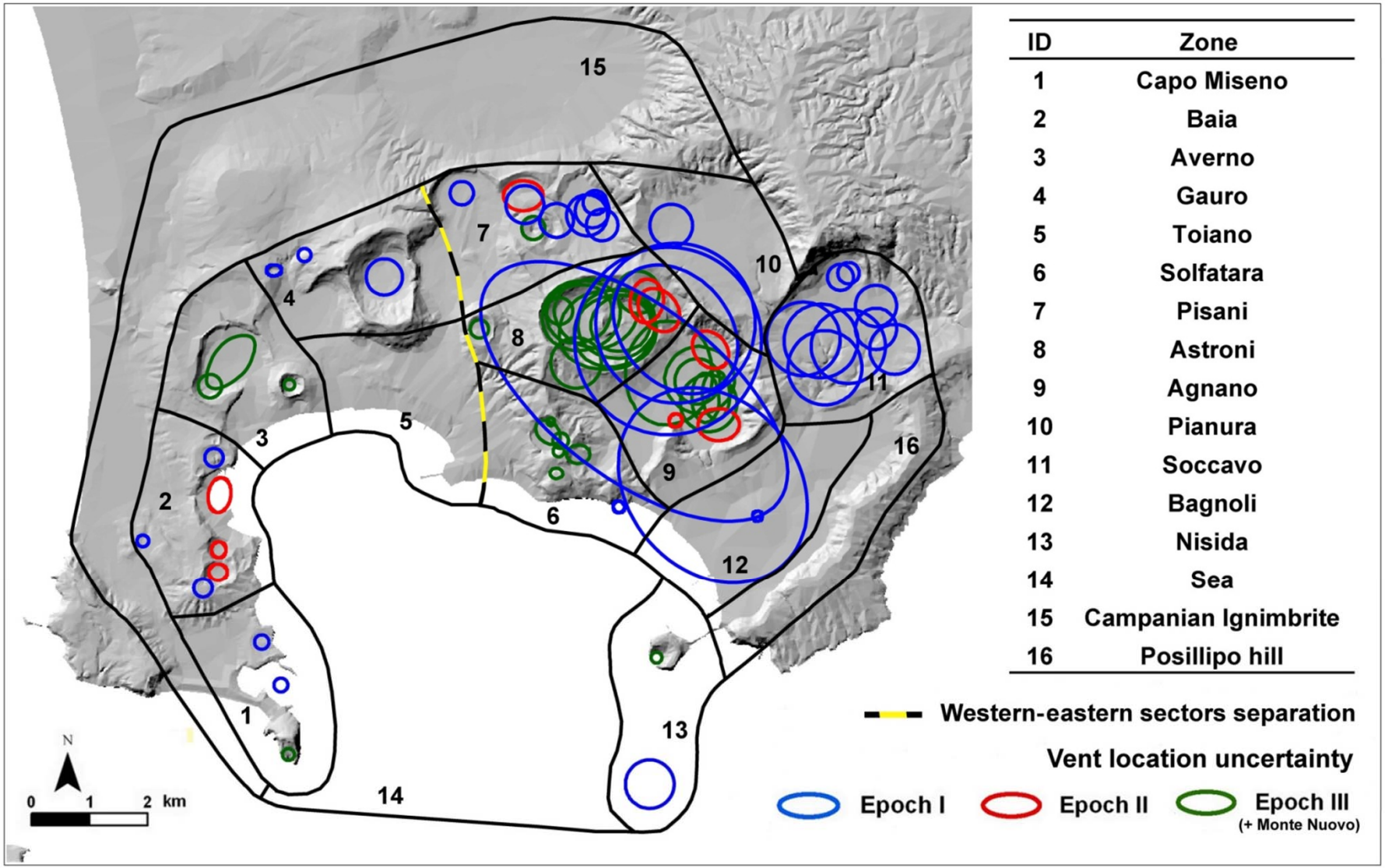

ID	Zone
1	Capo Miseno
2	Baia
3	Averno
4	Gauro
5	Toiano
6	Solfatara
7	Pisani
8	Astroni
9	Agnano
10	Pianura
11	Soccavo
12	Bagnoli
13	Nisida
14	Sea
15	Campanian Ignimbrite
16	Posillipo hill

Fig 8. Partitioning of the caldera in 16 zones. The colours of the ellipses correspond to the epoch of activity.
The yellow dashed line separates eastern and western sectors.

We convolved a two dimensional symmetric **Gaussian kernel** with the uniform probability measures enclosed in the uncertainty ellipses (e.g. Connor and Hill 1995; Mazzarini et al. 2003).
This produced a simplified **map of vent opening** based only on the past vents locations (Fig a).

We got consistent results which include more geological information, assuming uniform probability inside each **zone of the partition** in proportion with the number of ellipses contained (Fig b).
Separated maps have been produced for each epoch of activity, to combine them with different weights.

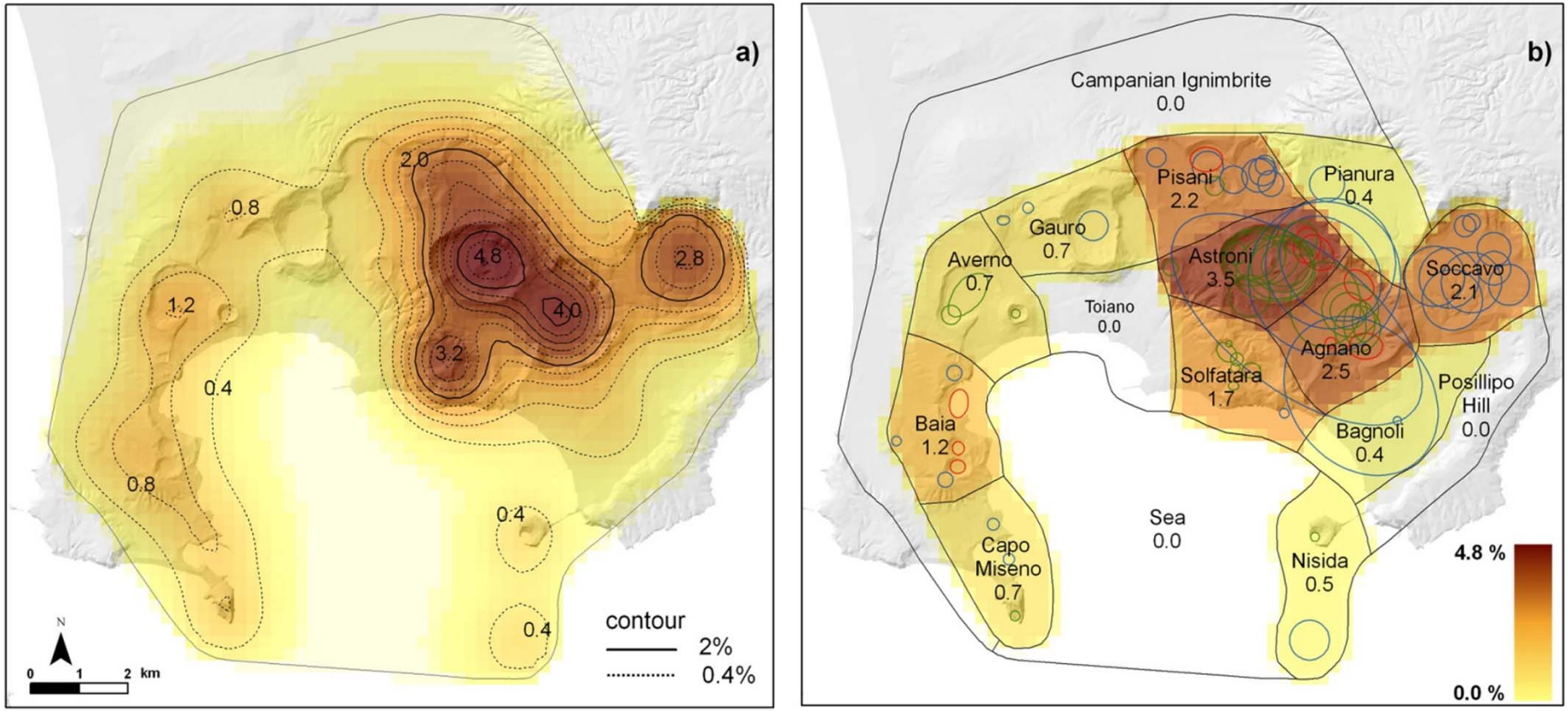

Fig 9. Density distribution of the probability of vent opening obtained using the past vent location data by: (a) kernel density estimation and (b) partitioning of the caldera in 16 homogeneous zones.
Values reported in the different subareas and on the contours indicate the percentage probability of vent opening per km^2.

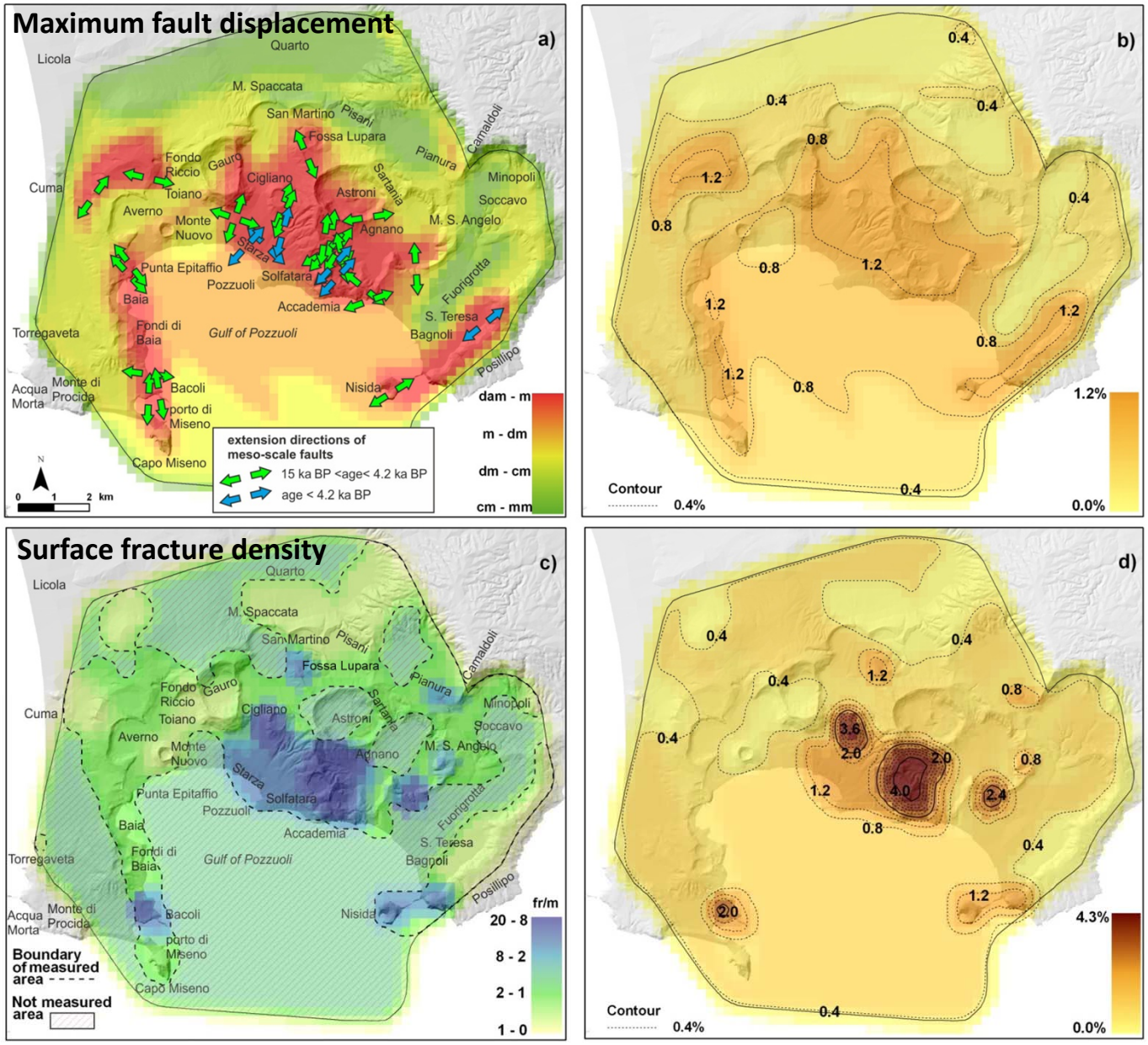

Other probability maps concern the structural features.
(e.g. Vitale and Isaia 2014)

The **faults map** shows the value of density of fault displacement taking into account the historical deformation patterns.

The **fractures map** shows the value of density of fracturation, as number of fractures per meter, obtained from discrete sampling.

Fig 10. (a) Maximum fault displacement in the caldera, with extensional directions. The colour levels correspond to different orders of magnitude. (c) Surface fracture density in the caldera. Values of density range between about 1 and 20 fr/m. Wide areas were not measured (dashed areas), and the average value of the measured zone was assumed. (b-d) Density distributions of the probability of vent opening obtained normalizing the values.

Performance based expert judgement

To make more robust the choice of the weights to give to the geological features and of the uncertainty associated, some **structured and performance based elicitation sessions** have been performed. (e.g. Aspinall 2006, Aspinall 2010, Flandoli et al. 2011)

Several elicitation sessions, involving **8 experts** with different volcanological backgrounds were carried out through **meetings** and also email consultations.

We followed two informed questionnaires:

- **The seed (or calibration) questions,** with known answers.
- **The target questions**

For each question (seed or target), the experts express their views as the values of **the 5th, 50th and 95th percentiles** of a 'primitive' probability measure representing their uncertainty.

The seed questions were about carefully researched aspects of Campi Flegrei volcanism, other Italian volcanoes, and about explosive volcanism in general.

The answers to the seed questions are adopted for **scoring the experts'** uncertainty estimation performances.

The answers to the **questions of interest** (target) were combined using the obtained scores, and the combination defined a new virtual expert: the **global Decision Maker (DM)**.

We computed three different **DM** using three different methods with different approaches:

- the **Cooke Classical Model (CM)**
- the **Expected Relative Frequency model (ERF)**
- an **Equal Weights pooling (EW)** of the experts' uncertainty densities

The performance based methods adopt different **performance scores, 'primitive' distributions and pooling rules** for combining the responses.

Expert / EJ method	*Expert 1*	*Expert 2*	*Expert 3*	*Expert 4*	*Expert 5*	*Expert 6*	*Expert 7*	*Expert 8*
Classical Method	3.2%	0.0%	0.0%	0.0%	6.8%	0.0%	89.9%	0.1%
Expected Relative Frequency	11.9%	7.8%	7.3%	8.8%	19.4%	13.4%	20.9%	10.5%
Equal weights	12.5%	12.5%	12.5%	12.5%	12.5%	12.5%	12.5%	12.5%

Tab 1. Performance scoring percentages assuming the different scoring rules.

The Cooke classical method uses maximal entropy probability measures, uniform in each inter-quantile range.

The performance score is the product of two values:

Calibration score: likelihood that the true results correspond to the expert distributions.
It could be considered as a statistical accuracy.

Information score: average relative information w.r.t. a uniform distribution.
It penalizes too large uncertainty ranges.

The ERF method uses triangular distributions, with the 50th percentile used as the vertex of the triangle.

The performance score adopted is:

Expected relative frequency: expectation of the frequency of random answers which fall in a selected interval around true values.
It could be assumed as a point-wise accuracy.

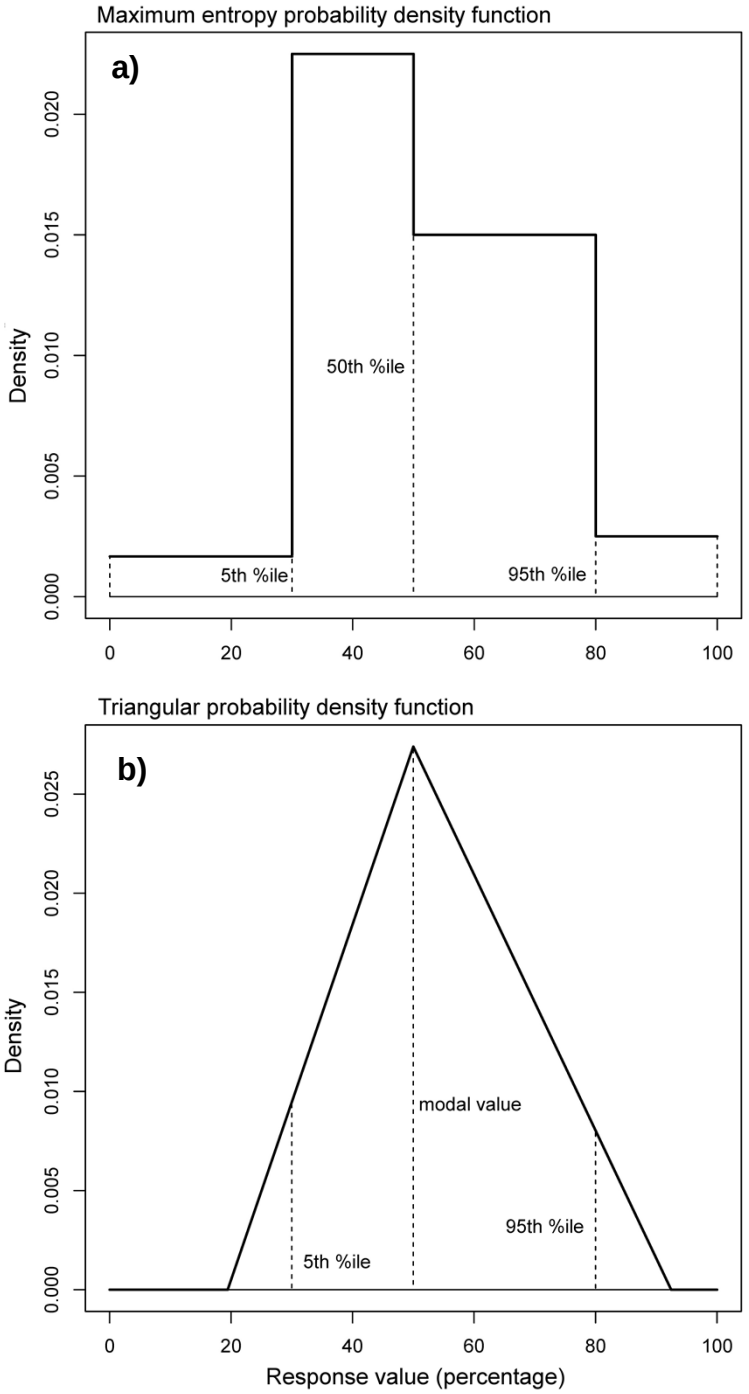

Fig 11. Examples of 'primitive' probability distributions for an expert response equal to [30% - 50 % - 80%].

To simplify the quantification of the weights of each spatial distribution, we did not ask them directly.

A **simple hierarchical logic tree** has been defined: most of the **target questions** quantify the **relative importance**, or relevance, of one variable or feature of the system versus others.

Other relevant questions were about the estimation of the **number of 'lost vents'** in each epoch of activity.

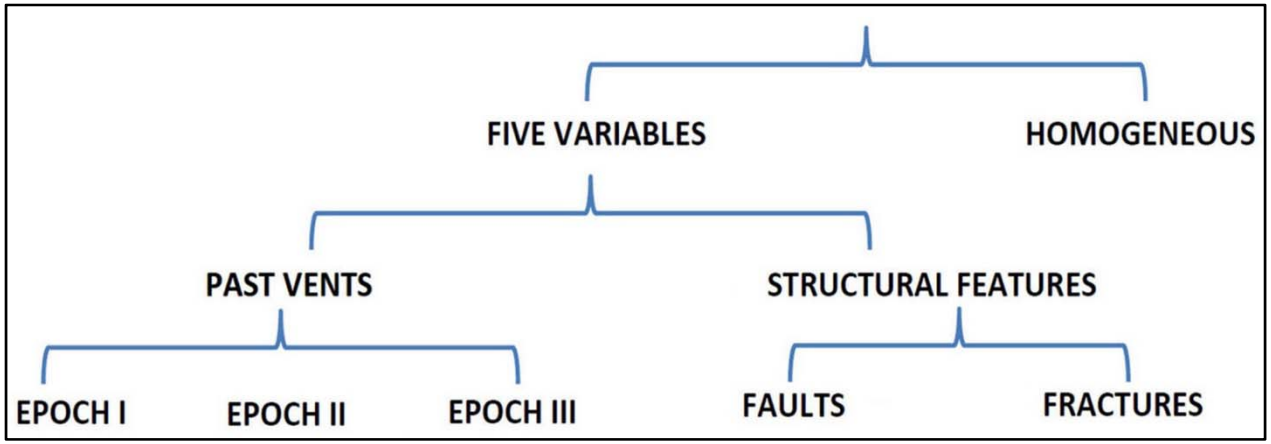

Fig 12. Hierarchical logic tree structure associated to the target questions queried during the elicitation sessions.

We followed a **Monte Carlo simulation approach** on the single branch weight estimates, **multiplying the single estimates over each branch** of the logic tree for obtaining the probability distribution of the weights $\alpha = (\alpha_i)_{i=1,\ldots,d}$.

Tab 2. Probability percentages of the mean and 5*th* and 95*th* percentiles of the weights with respect to the CM, ERF and EW methods.

Variable/ Method	*Vents Epoch I*	*Vents Epoch II*	*Vents Epoch III*	*Lost vents*	*Faults*	*Fractures*	*Homog. map*	**Statistics**
CM	*6.3*	*1.3*	*10.2*	*3.3*	*8.1*	*5.4*	*6.3*	*5%ile*
	16	***4.5***	***20.4***	***5.9***	***16.4***	***11.9***	***24.9***	***Mean***
	26.7	*8.7*	*33.3*	*9*	*26.6*	*20.4*	*42.4*	*95%ile*
ERF	*9.5*	*2.2*	*14.7*	*4.2*	*10.2*	*7*	*8.7*	*5%ile*
	16.4	***4.8***	***22.5***	***6.3***	***16.5***	***12.3***	***21.3***	***Mean***
	24	*7.6*	*31.6*	*8.8*	*23.9*	*18.6*	*31.1*	*95%ile*
EW	*6.3*	*1.5*	*7.6*	*3.4*	*5.3*	*4.3*	*6.5*	*5%ile*
	17.7	***4.6***	***19.3***	***6.7***	***13.8***	***12***	***25.9***	***Mean***
	30.5	*9.3*	*33.8*	*11*	*24.3*	*22*	*45.4*	*95%ile*

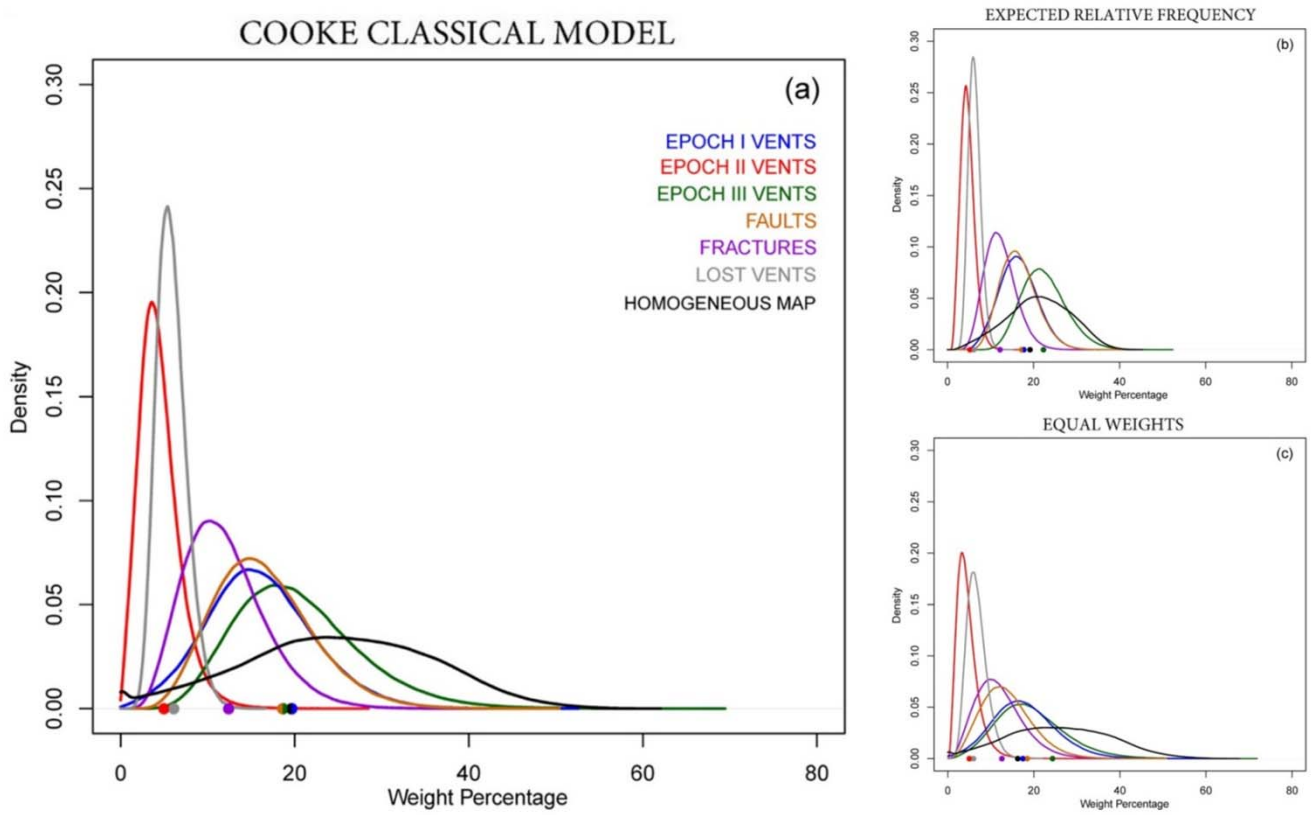

Fig 13. Pdfs of the weights from the elicitation models assumed, i.e., (a) Cooke CM, (b) ERF model, and (c) EW model.

Along the x axis are also reported as coloured dots the estimates obtained by using just the best guess (central) values of the experts.

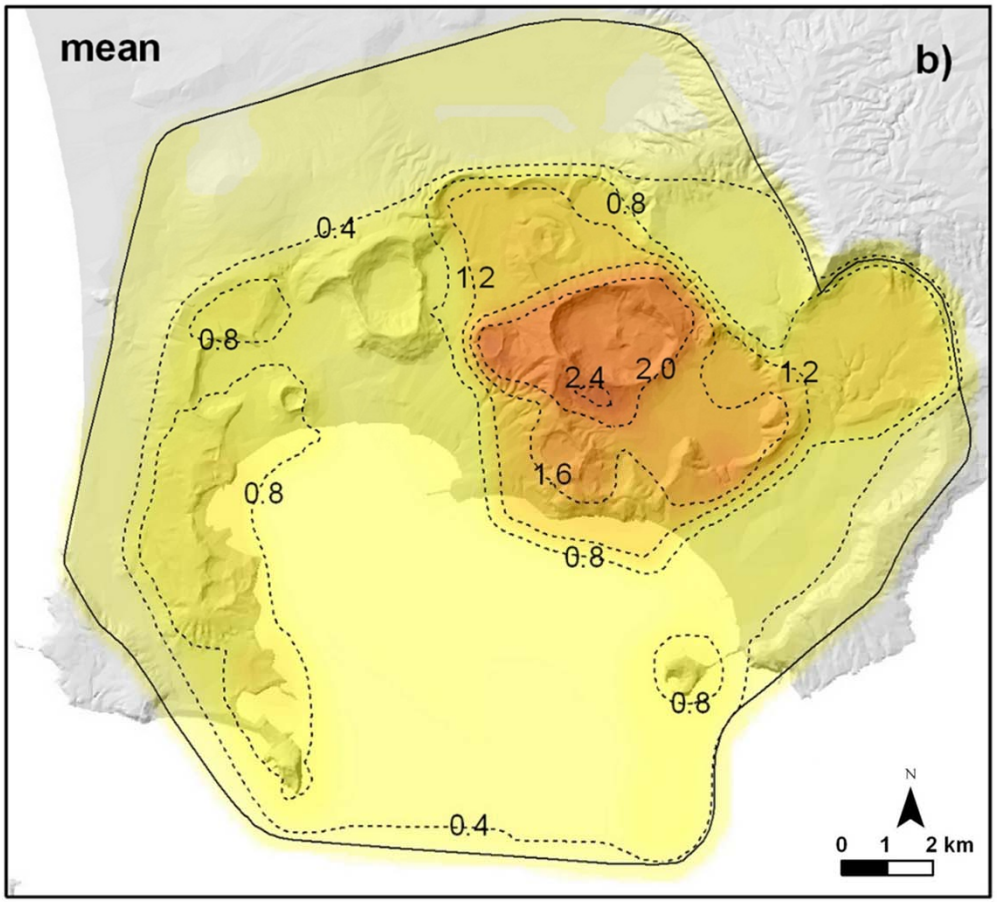

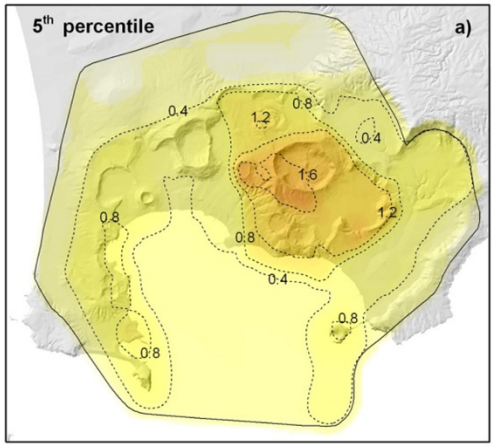

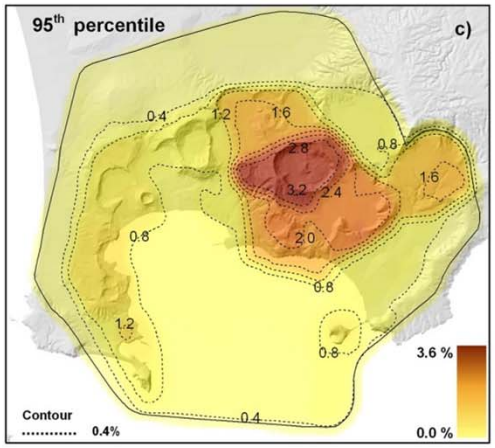

Fig 14. Probability density maps of new vent opening location.

(a), (b) and (c) refer to the 5*th* percentile, mean and 95*th* percentile values of the density, with respect to epistemic uncertainty.

Contours and colours indicate the percentage probability of vent opening per km^2 conditional on the occurrence of an eruption.

Results have shown evidence for a main **high probability** region in the **central-eastern portion of the caldera**. Significantly lower **secondary largest** are found to exist in both the **eastern and western parts of the caldera**.

Nevertheless the spatial distribution of vent opening position **probability is widely dispersed** over the whole NYT caldera, including the offshore portion.

We accompany the probabilities with **quantified uncertainty estimates** which are indicative, typically, of spreads ±30% on the local mean value.

PART II

Pyroclastic density current invasion hazard maps

In our analysis, we designated the **areas invaded (inundated) by the past PDCs** as a variable representative of the distribution of the next PDC magnitudo. We focused on the more dilute part of the flows (surge-like).

ID	PDC Deposit - Epoch I	Area (km^2)
1	Bellavista Volcano	3.9
2	Mofete Volcano	2.1
3	Gauro Volcano	16.1
4	Santa Teresa Volcano	0.9
5	La Pietra Volcano	2.6
8	Torre Cappella Volcano	1.0
11	Soccavo 1 Tephra	190.5
13	Pomici Principali Tephra	129.2
14	Paleo Pisani 2 Tephra	37.7
16	Soccavo 2 Tephra	75.8
17	Soccavo 3 Tephra	147.5
20	Soccavo 4 Tephra	180.2
21	Paleo San Martino Tephra	37.3
22	Minopoli 2 Tephra	113.6
23	Soccavo 5 Tephra	66.2
25	Pisani 2 Tephra	21.1
28	Montagna Spaccata Tephra	3.0
30	Pisani 3 Tephra	3.0
32	Bacoli Volcano	1.1
33	Porto Miseno Volcano	0.7

ID	PDC Deposit - Epoch II	Area (km^2)
2	Fondi di Baia Tephra	15.7
3	Sartania 1 Tephra	40.7
5	Costa San Domenico Tephra	16.9
6	Pigna San Nicola Tephra	8.0
7	Sartania 2 Tephra	27.0
8	San Martino Tephra	19.7

ID	PDC Deposit - Epoch III	Area (km^2)
2	Agnano 2 Tephra	17.1
3	Averno 1 Tephra	27.0
4	Agnano 3 Tephra	68.0
5	Cigliano Tephra	28.3
7	Capo Miseno Volcano	1.1
8	Monte Sant'Angelo Tephra	43.8
9	Paleoastroni 1 Tephra	18.1
10	Paleoastroni 2 Tephra	5.4
11	Agnano Monte Spina Tephra	312.5
18	Solfatara Tephra	8.7
19	Averno 2 Tephra	24.8
20	Astroni 1 Tephra	39.7
21	Astroni 2 Tephra	19.1
22	Astroni 3 Tephra	41.1
23	Astroni 4 Tephra	60.4
24	Astroni 5 Tephra	29.1
25	Astroni 6 Tephra	26.9
26	Astroni 7 Tephra	10.2
27	Fossa Lupara Tephra	8.9
28	Nisida Tephra	4.7
29	Monte Nuovo Tephra	5.7

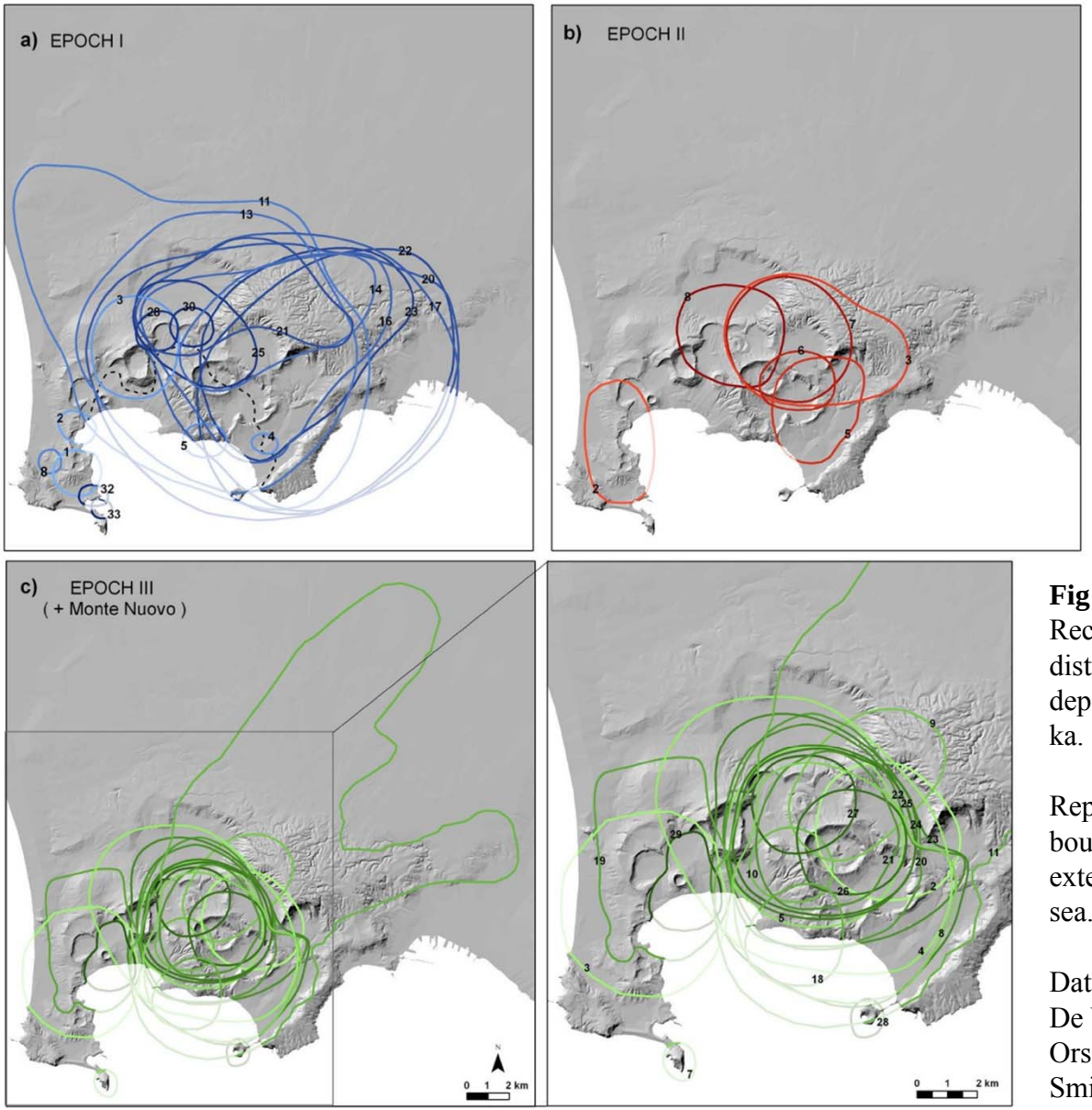

Fig 17.
Reconstruction of the distribution of PDC deposits of the last 15 ka.

Reported deposit boundaries were extended over the sea.

Data modified from De Vita et al. 1999; Orsi et al. 2004; Smith et al. 2011.

Again the **identification**, and where possible the **quantification**, of some of the main **sources of epistemic uncertainty** is a key aspect.

In this case:

• the **radial underestimation error** of deposit boundaries (elicited between 150m and 1000m);

• the **lost PDCs** invasion areas (randomly extracted following the known invasion areas);

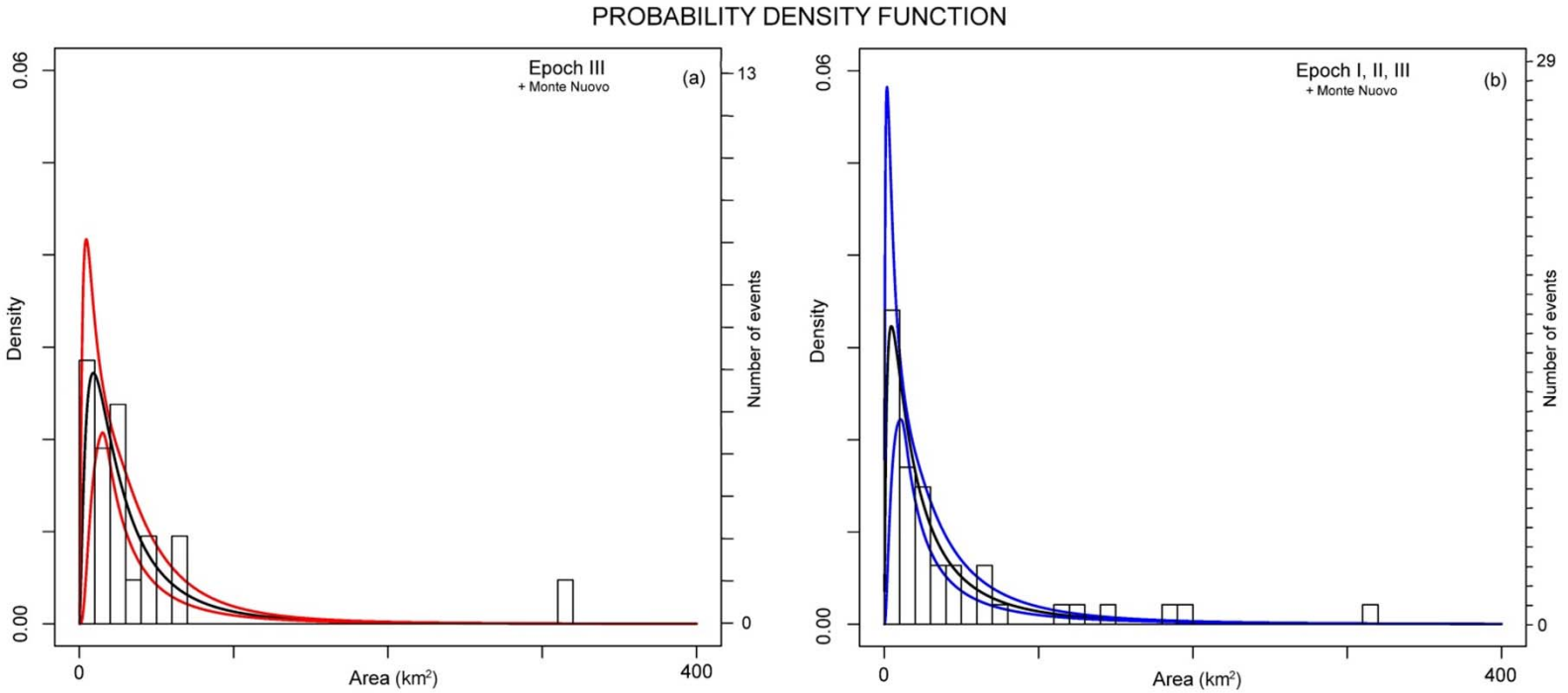

Figure 18. Histograms of the PDC invasion areas and probability density functions for the invasion areas.

The black curve is the mean and the coloured curves are the 5*th* and 95*th* uncertainty percentiles

We adopted a maximum likelihood lognormal distribution, but also Power law or Weibull were considered.

We based the hazard assessment on the construction of a set function *F* such that *F(x,y)* represents the set invaded by a PDC propagating from a vent located in *x* with an area extension *y*.

The dynamics of the PDC is described as the **collapse of a constant volume of dense fluid** in a lighter one and on a flat surface (e.g. Huppert and Simpson 1980; Dade and Huppert 1996; Harris et al. 2002).

Dynamical system of the front position 'Box Model'

$$\begin{cases} u = \dfrac{dl}{dt} = Fr(g_p \phi h)^{1/2}, & \text{(Von Kàrman, 1940)} \\ \dfrac{d\phi}{dt} = -w_s \dfrac{\phi}{h}, & \text{(Particles deposition)} \\ l^2 h = V. & \text{(Geometric condition) (axisymmetric)} \end{cases}$$

$$g_p = \frac{\rho_p - \rho_a}{\rho_a} g \quad \text{(Reduced gravity)}$$

Different geometric constrains, i.e. rectangular, lead to different solution.

We calculated the **relationship between front position and time** as a function of initial conditions.

$$l(t) = [\tanh(t/\tau)]^{1/2} \, l_{max}$$

$$\tau = \left(Fr^{-1}(g_p \phi_0 V)^{-1/2} l_{max}^2\right)/2$$

$$l_{max} = \left(8\phi_0^{1/2} g_p^{1/2} V^{3/2} w_s^{-1} Fr\right)^{1/4}$$

w_s is the settling velocity of the particles
ϕ_0 is the initial volume fraction of the particles
V is the constant volume (divided by π)

Fr is the Froude number, representing the relation between inertial and gravitational forces.

It is possible to calculate a function *K* such that $K(r, l_{max})$ is the kinetic energy of a PDC with maximum run-out l_{max} at a distance *r* from the vent.

$$K(r, l_{max}) = \frac{1}{2}\left[\frac{C l_{max}^{1/3}}{\hat{r}\cosh^2 artanh(\hat{r}^2)}\right]^2$$

$$\hat{r} = r/l_{max}$$

$$C = \left(F r^2 w_s \phi_0 g_p\right)^{1/3}/2$$

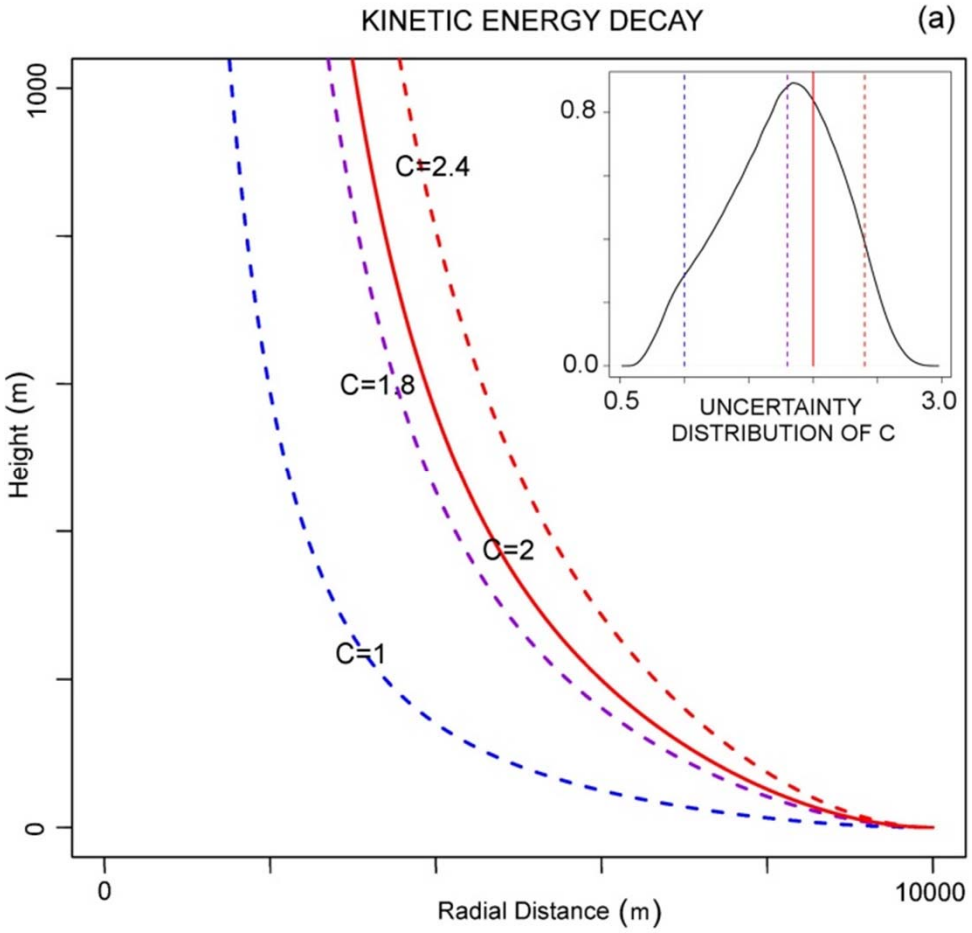

We compared the **kinetic energy** of the flow front with the height of the **topographic relief** potentially reached/overcome, finding the set of the points which the current has **enough energy** to reach.

This PDC invasion model was applied in an **inverse mode,** repeated for each sample of a Monte Carlo simulation varying vent location and PDC areal size.

Fig 19. (a) Example of decay of radial flow head kinetic energy as a function of distance from the source. An example of a probability density function for the C parameter is shown.

Curves refer to a flow run-out of 10 km and to values of the C.

The PDC invasion hazard maps with uncertainty

The mean and percentile **PDC invasion hazard values** with respect to the epistemic uncertainty, were mapped in each point of the Campi Flegrei area.

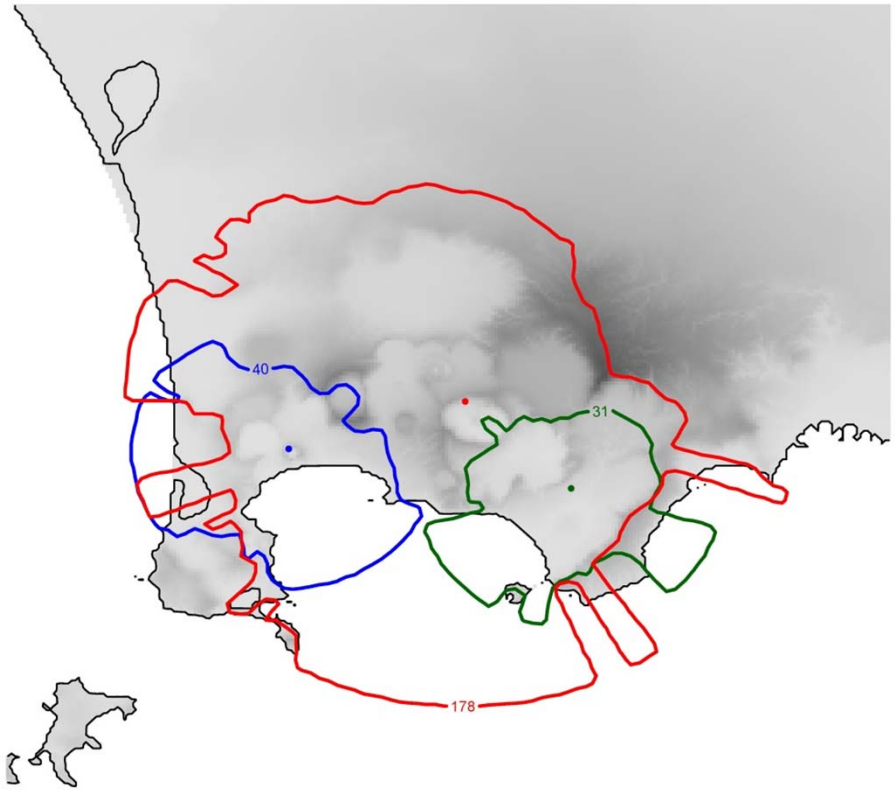

We combined:
- the spatial probability **map of new vent opening**,
- the probability distribution of **PDC invasion areas,**
- by using the **simplified propagation model.**

The inverse mode adopted strongly linked the PDC hazard estimates to the past deposits extents but required to numerically **invert the propagation model** during each simulation.

Fig 20. Examples of single PDC propagations, assuming different vent locations (the colored points) and areal sizes in km^2 (the numbers reported on the curves).

All our maps relate solely to the **probability of invasion** by PDCs and not to the distributions of specific hazard variables.

It was assumed that a future PDC episode will originate in the **onland portion** of the caldera because source conditions would be fundamentally and significantly different in the case of an underwater vent.

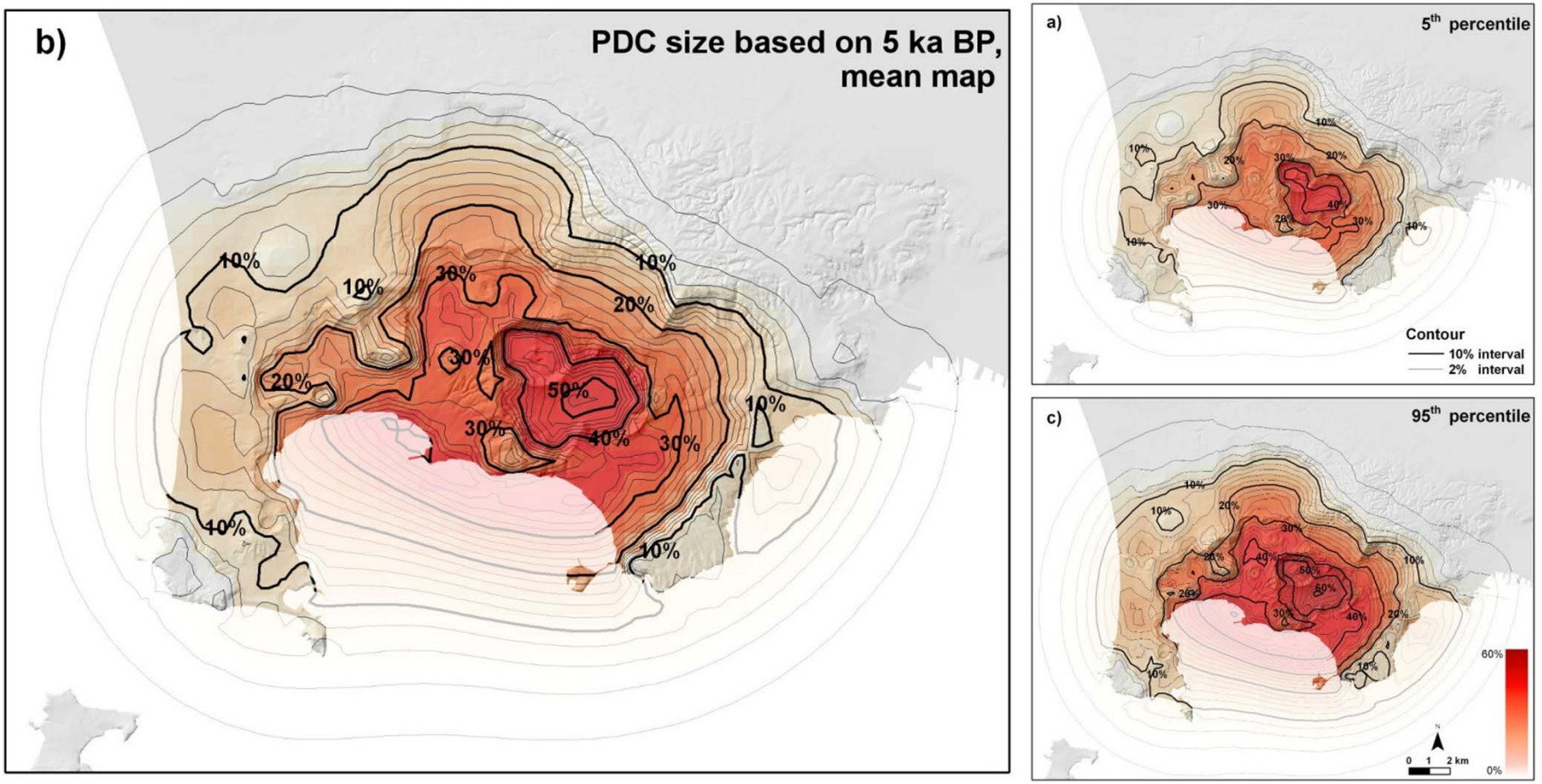

Fig 21. PDC invasion probability maps based on invasion areas of the last 5 ka, a single vent per eruption, located in the on-land part of the caldera. Contours and colours indicate the percentage probability of PDC invasion conditional on the occurrence of an explosive eruption.

Mean invasion probabilities above 5% are calculated over the **whole CI caldera**, with peak values exceeding 50% in the Agnano plain.

Mean probabilities above 10% are also computed in some areas **outside** the caldera, across Posillipo hill.

Uncertainty ranges affecting invasion probabilities inside the caldera lay between ±15 and ±35% of the local mean value; wider uncertainties are found outside the caldera, with an average above ±50%.

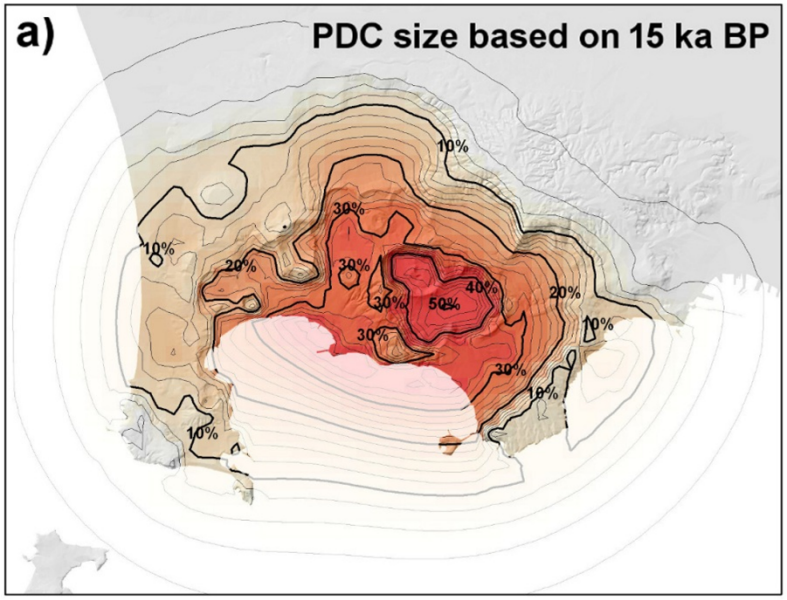

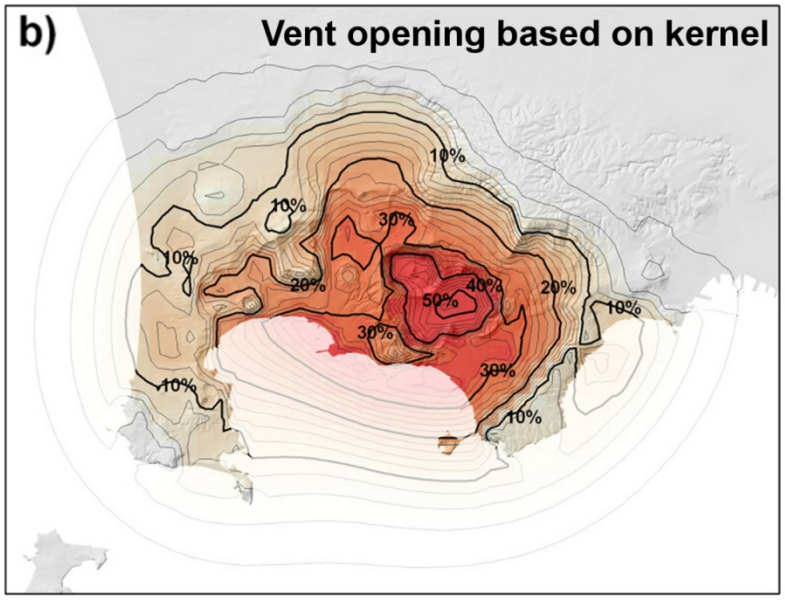

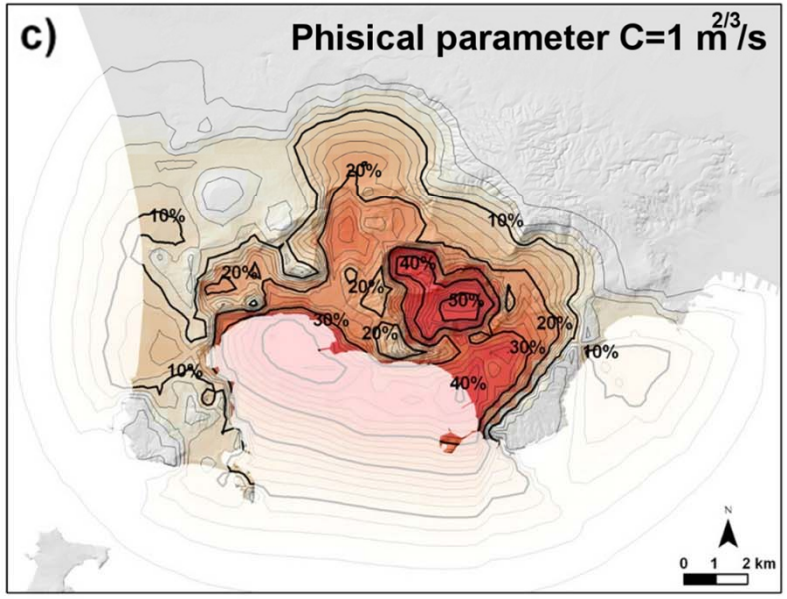

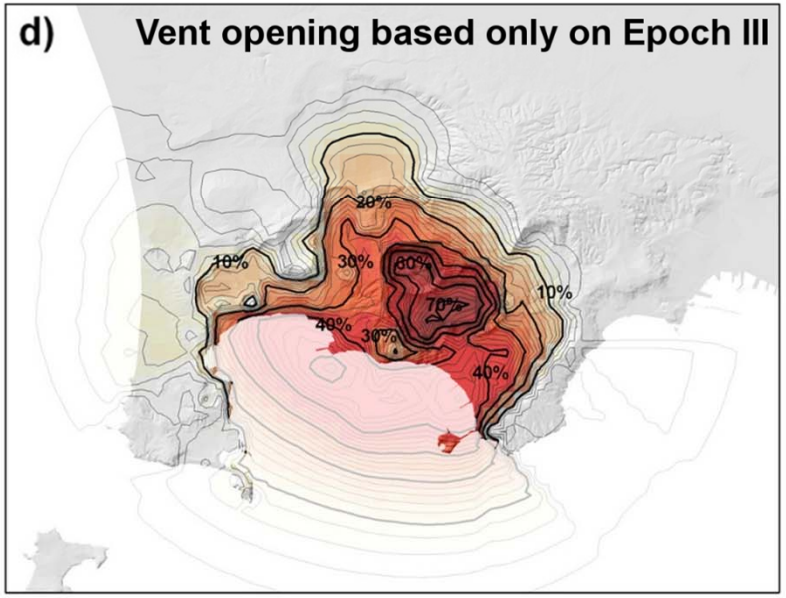

Fig 22. (a) PDC invasion hazard mean probability map with PDC size based on 15 ka record;

(b) assuming vent opening maps based on kde;

(c) assuming a value of parameter C equal to 1 $m^{2/3}/s$ instead of 2 $m^{2/3}/s$;

(d) considering only the vent locations of the events of last 5 ka.

Contours and colours indicate the percentage probability of PDC invasion conditional on the occurrence of an explosive eruption from a single vent located on-land.

As it emerges from the comparisons, despite some significant differences observed locally in specific areas of the caldera, the main findings about the spatial distribution of PDC invasion probabilities remain largely valid.

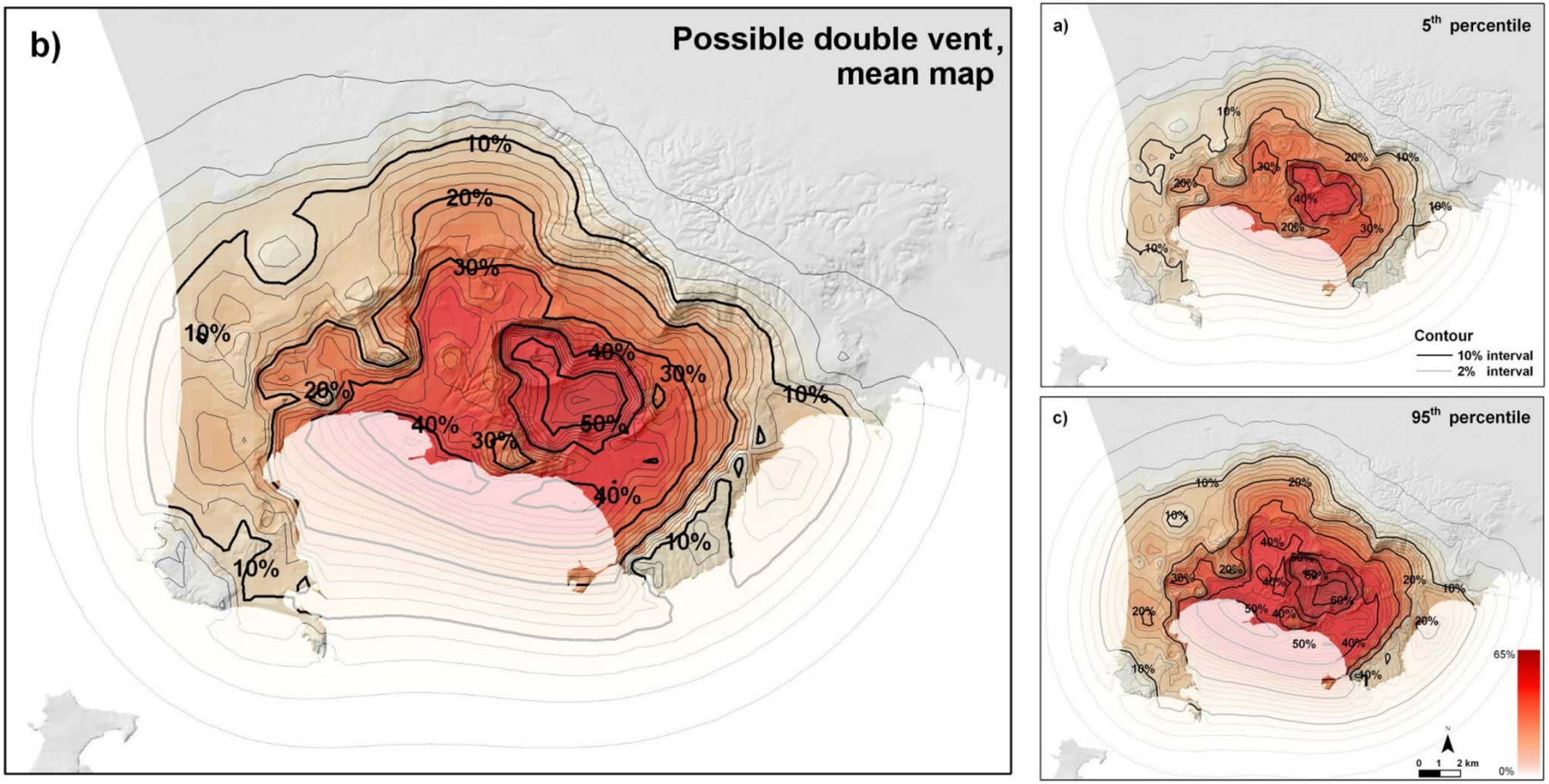

Fig 23. PDC invasion probability maps based on invasion areas of the last 5 ka, possibly originating from two simultaneous vents, both located in the on-land part of the caldera.

The probability of a double event is [5% - 10% - 25%], distance between simultaneous vents of [1 - 4.7 - 10] km. Contours and colours indicate the percentage probability of PDC invasion conditional on the occurrence of an explosive eruption.

It is produced a slightly wider inundation hazard, with a general increase of probability values of about +2% compared to the case of single vent.

PART III

Time-space model for the next eruption

This part of the study included two phases:
1) A probability model for epistemic uncertainty on past record, concerning the **uncertainty estimation** on the sequence of times, the location and the erupted volume of past events.

2) A probability model for the **representation and replication** of the main eruptive activity features in time-space, such as the vent clustering, and incorporating the effects of the sources of epistemic uncertainty considered.

The two models are linked through a nested Monte Carlo simulation by assuming to calculate the parameters of model (2) that **maximize the likelihood** of each sample of model (1).

The approach followed relies on the **mathematical modeling** of the past record without assuming any physical model describing the deep-crustal processes.

Probability model for epistemic uncertainty on past record

We based on the data available in Smith et al. 2011, including some updates.

In the eruption record there are 3 classes of events:

A) with **datation only**;

B) with **sequence order only**;

C) with **both order and date**;

Events in (A) and (C) were sampled with **symmetrical triangular distributions** with the assumed percentiles.

Events in (B) were sampled **uniformly and independently** inside intervals consistent with the sequence.

Uncertainty affecting the estimated volumes is assumed equal to ±50%, consistently with recent literature (e.g. Klawonn et al. 2014)

EPOCH I

ID	Name	Time [a]		VDRE [hm3]			E/W	Zone
		2.5%ile	97.5%ile	5%ile		95%ile		
1	Bellavista	-	-	10	-	100	W	2
2	Mofete	-	-	10	-	100	W	2
3	Gauro	12721	15511	250	500	750	W	4
4	Santa Teresa	-	-	10	-	100	E	12
5	La Pietra	-	-	10	-	100	E	6
6	La Pigna 1	12749	13110	10	-	100	E	11
7	La Pigna 2	-	-	10	-	100	E	11
8	Torre Cappella	-	-	10	-	100	W	2
9	Minopoli 1	-	-	10	-	100	E	11
10	Paradiso	-	-	10	-	100	E	11
11	Soccavo 1	-	-	250	500	750	E	11
12	Gaiola	-	-	10	-	100	E	13
13	Pomici Principali	11915	12158	425	850	1275	E	8 - 9 - 10
14	Paleo Pisani 1	-	-	10	-	100	E	7
15	Paleo Pisani 2	-	-	100	-	300	E	7
16	Soccavo 2	-	-	10	-	100	E	11
17	Soccavo 3	-	-	10	-	100	E	10
18	S4s3_1	-	-	100	-	300	E	8 - 9 - 10
19	S4s3_2	-	-	10	-	100	E	8 - 9 - 10
20	Soccavo 4	-	-	100	-	300	E	11
21	Paleo San Martino	-	-	10	-	100	E	7
22	Minopoli 2	-	-	10	-	100	E	11
23	Soccavo 5	-	-	10	-	100	E	11
24	Pisani 1	-	-	100	-	300	E	7
25	Pisani 2	-	-	100	-	300	E	7
26	Fondo Riccio	-	-	0	-	10	W	4
27	Concola	-	-	0	-	10	W	4
28	Montagna Spaccata	-	-	10	20	30	E	7
29	Pignatiello 1	-	-	10	-	100	E	6 - 7 - 8 - 9 - 12
30	Pisani 3	10516	10755	10	-	100	E	7
31	Casale	-	-	10	-	100	E	6 - 9 - 12
32	Bacoli	11511	14154	100	200	300	W	1
33	Porto Miseno	10347	12860	10	-	100	W	1

EPOCH II

ID	Name	Time [a]		VDRE [hm3]			E/W	Zone
		2.5%ile	97.5%ile	5%ile		95%ile		
1	Baia	-	-	0	-	10	W	2
2	Fondi di Baia	9525	9695	20	40	60	W	2
3	Sartania 1	9500	9654	10	-	100	E	8
4	Monte Spina lava dome	-	-	0	-	10	E	9
5	Costa San domenico	-	-	10	-	100	E	9
6	Pigna San Nicola	9201	9533	100	-	300	E	9
7	Sartania 2	-	-	10	-	100	E	8
8	San Martino	9026	9370	25	50	75	E	7

EPOCH III

ID	Name	Time [a]		VDRE [hm3]			E/W	Zone
		2.5%ile	97.5%ile	5%ile		95%ile		
1	Agnano 1	5266	5628	10	20	30	E	9
2	Agnano 2	-	-	5	10	15	E	9
3	Averno 1	5064	5431	10	-	100	W	3
4	Agnano 3	-	-	95	190	285	E	9
5	Cigliano	*	*	25	50	75	E	8
6	Pigniatiello 2	*	*	10	20	30	E	9
7	Capo Miseno	3259	4286	10	20	30	W	1
8	Monte Sant'Angelo	4832	5010	100	-	300	E	9
9	Paleoastroni 1	4745	4834	25	50	75	E	8
10	Paleoastroni 2	4712	4757	100	-	300	E	8
11	Agnano Monte Spina	4482	4625	425	850	1275	E	8 - 9
12	St. Maria delle Grazie	4382	4509	10	-	100	E	6
13	Olibano lava dome	*	*	0	-	10	E	6
14	Paleoastroni 3	-	-	10	20	30	E	8
15	Solfatara lava dome	*	*	0	-	10	E	6
16	Olibano tephra	*	*	10	-	100	E	6
17	Accademia lava dome	-	-	0	-	10	E	6
18	Solfatara	4181	4386	15	30	45	E	6
19	Averno 2	**	**	35	70	105	W	3
20	Astroni 1	4153	4345	30	60	90	E	8
21	Astroni 2	-	-	10	20	30	E	8
22	Astroni 3	-	-	80	160	240	E	8
23	Astroni 4	-	-	70	140	210	E	8
24	Astroni 5	-	-	50	100	150	E	8
25	Astroni 6	-	-	60	120	180	E	8
26	Astroni 7	4098	4297	35	70	105	E	8
27	Fossa Lupara	3978	4192	10	20	30	E	7
28	Nisida	3213	4188	10	20	30	E	13

Tab 3. Record of times, erupted volumes and locations (eastern or western sectors and partition zones) of the events at CF during last 15 ka.

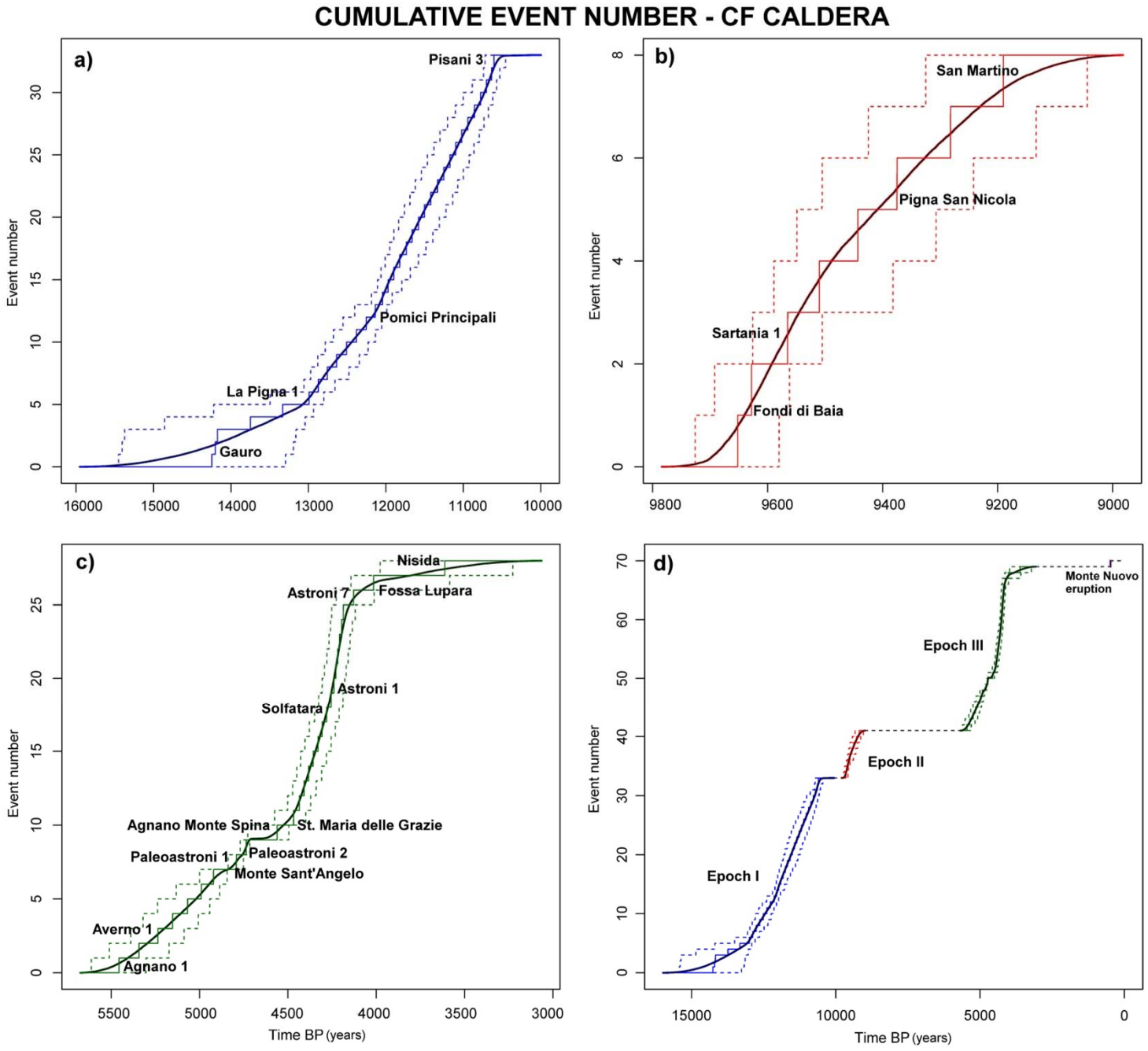

Fig 24. Event number as a function of time during Epoch I (a), Epoch II (b), Epoch III (c) and then during the entire record considered (d) (including Monte Nuovo).

Bold line is the mean value, narrow line is the 50th percentile and dashed lines are 5th and 95th uncertainty percentiles.

The labels correspond to the eruptions with both datation bounds and sequence place.

Intensification of the activity rate is quite evident after about ten events from the beginning of Epoch I and III.

The change in eruption rate seems to coincide with a **climatic eruption**.

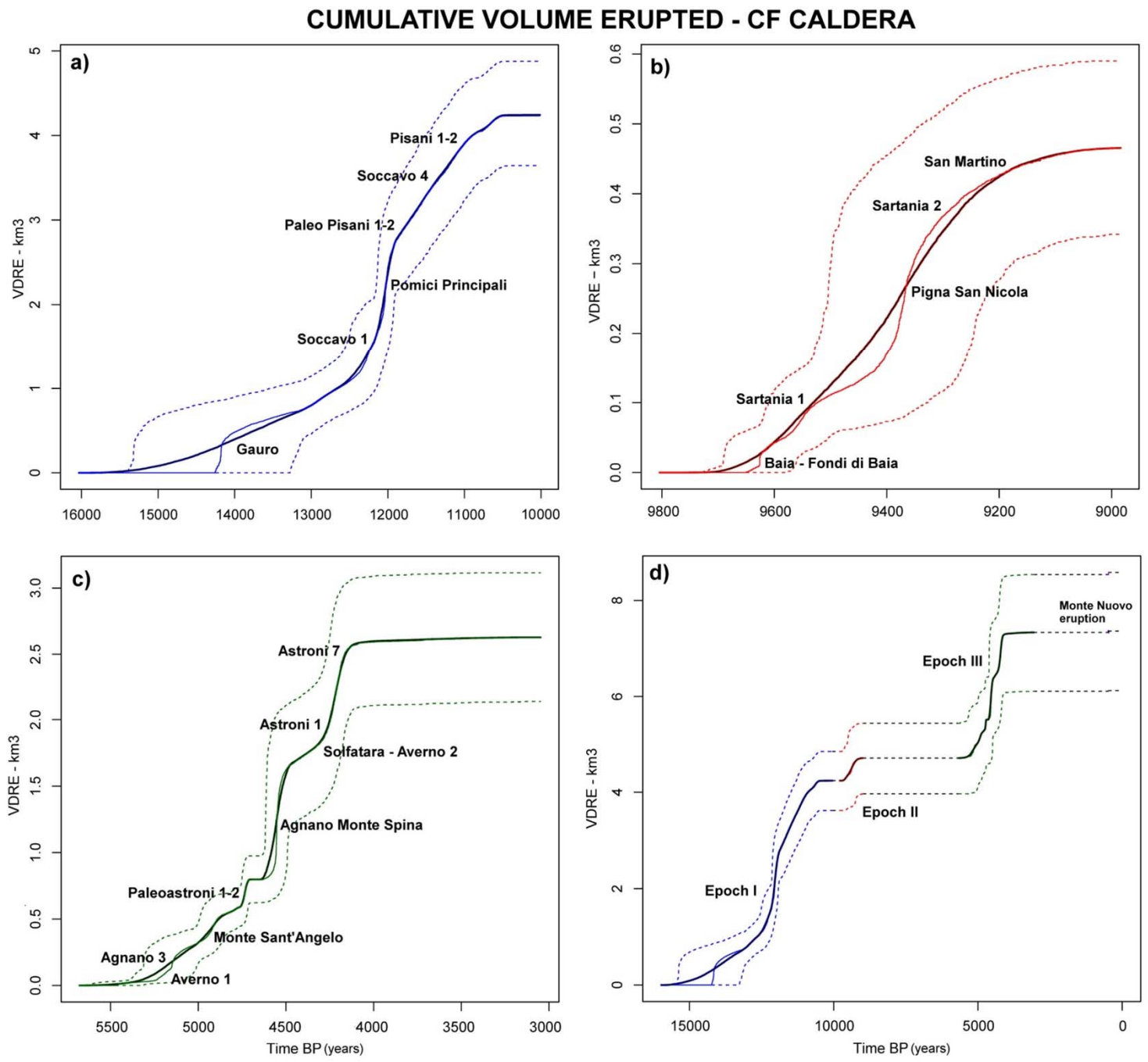

Fig 25. Cumulative volume erupted as a function of time during Epoch I (a), Epoch II (b), Epoch III (c) and then during the entire record considered (d) (including Monte Nuovo).

The labels correspond to the largest eruptions of each epoch.

Epoch II, 0.5 ±0.1 km^3, involved volumes 5 times smaller than Epoch III, 2.6 ±0.5 km^3, and even 8 times smaller than Epoch I, 4.2 ±0.7 km^3.

In Epoch III the estimates of the volume of Astroni sequence (7 events) are quite similar to the estimates of AMS (1 event).

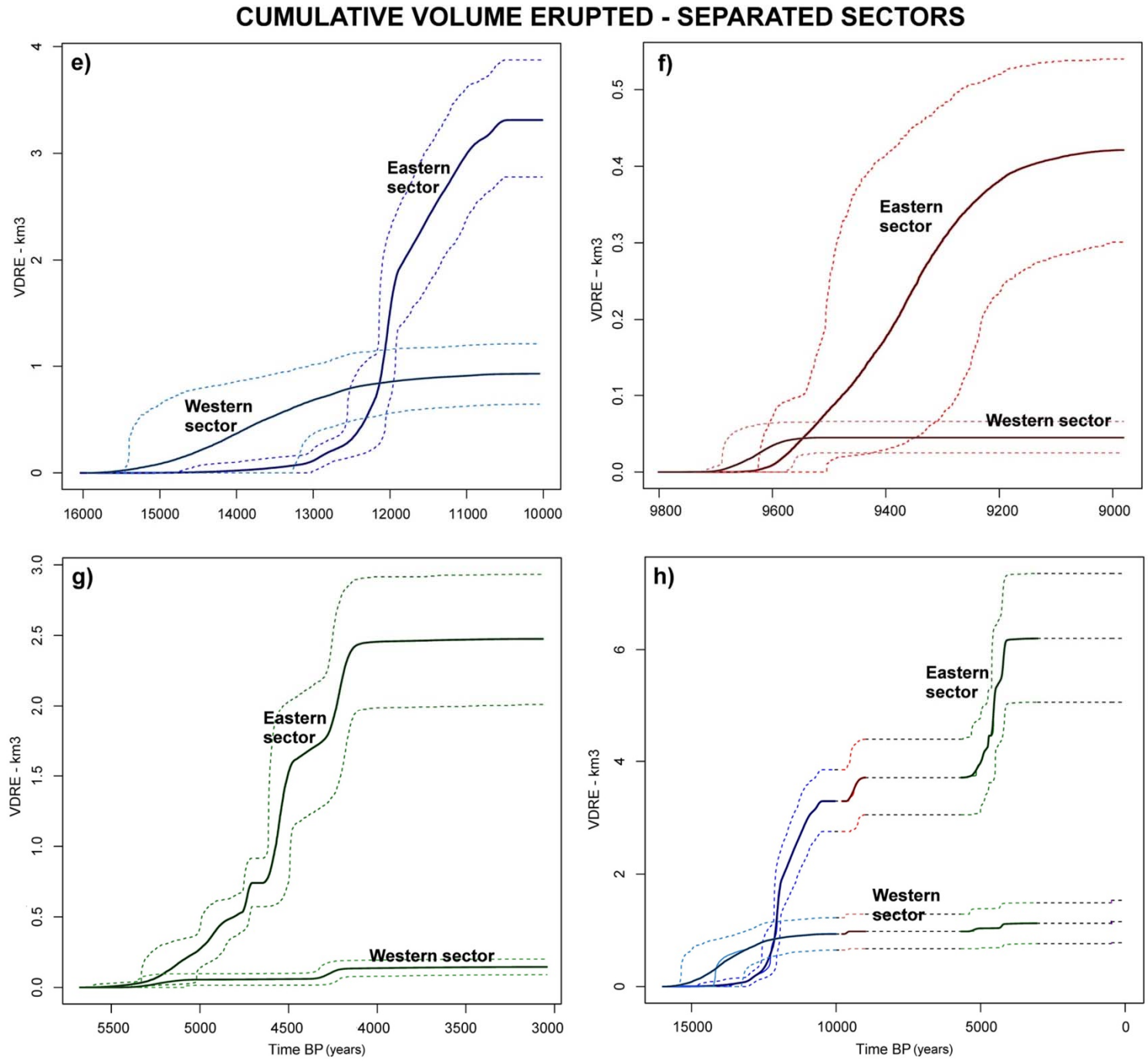

Fig 26. Cumulative volume erupted as a function of time during Epoch I (a), Epoch II (b), Epoch III (c) and then during the entire record considered (including Monte Nuovo) (d).

Separation between the eastern and the western sectors of the caldera.

The cumulative volumes erupted by the western part of the caldera, are remarkably **smaller** than by the eastern.

Activity in the western sector seems mainly associated to the **initial phases** of the eruptive epochs, compatible with considering the recent Monte Nuovo eruption as the **first one** of a new Epoch.

Probability model for the eruption pattern replication

The stochastic process Z which has been chosen for representing the eruptive events as a function of time belongs to the class of **Cox-Hawkes** multivariate counting processes.

Each component Z^l counts the number of events occurred in zone A_l of the caldera partition.

Cox-Hawkes generalize the class of **Poisson processes**, which sample the waiting times between events as independent identically distributed exponential random variables.

In general the intensity function λ of a counting process has the meaning of the **average density** of new events occurring in the selected time interval. Indeed the integral $\int\lambda dt$ gives the average number of events in the selected time interval.

The **Cox processes** assume their intensity function λ affected by uncertainty. They are doubly stochastic. (e.g. Jaquet et al. 2000; Jaquet et al. 2008)

Hawkes processes assume that their intensity function increases with a jump whenever an event occurs and decreases as time passes without any event occurring. They naturally **generate clusters**.
(e.g. Bebbington and Cronin 2011)

The **Cox-Hawkes processes** are both doubly-stochastic and self-exciting.

With multivariate Cox-Hawkes processes we assumed that each new eruption **self-excites** its zone, increasing the probability of additional eruptions nearby. Including the effects of **epistemic uncertainty** in the model.

For the Cox-Hawkes processes we have: $$\lambda^l(t,\omega) = \lambda_0^l(e) + \sum_{t_i^l(w)<t} [\varphi(e)](t - t_i^l(\omega))$$

Random intensity is the sum of a **constant term λ_0** (base rate) and of a time dependent random term that represents an **additional intensity** produced by each previous event.

The base rate represents the average density of new clusters (even of one point), while their additional intensity generates the offspring points.

φ is a positive decreasing function, representing self-excitement decay. It was assumed **exponential** and depending on two parameters. $$[\varphi(e)](s) = h(e)\exp(-k(e)s)$$

The parameters $\lambda^l{}_0(e)$, $k(e)$ and $h(e)$ are **conditional on the epistemic assumptions**, represented by e. We estimated them by a maximum likelihood procedure.

Indeed it is possible to calculate an **expression for the likelihood** of an eruption sequence of in zone *l,* before time *t*. $$L_l\left((t_i^l)_{i=1,\dots,n^l}, t\right) = \left(\prod_{i=1}^{n^l} \lambda^l(t_i^l)\right) \exp\left(-\int_0^t \lambda^l(s)ds\right)$$

This was implemented in a nested **Monte Carlo simulation** and repeated for each sample of the uncertainty.

From the maximum likelihood **parameters** on the three eruptive epochs it is obtained:

	Renewal time $1/\lambda_0$	Self-excitement decay	Mean offspring
Epoch I	[98 - 148 - 237] years	[60 - 658 - 1320] years	[0.14 - 0.30 - 0.43]
Epoch II	[43 - 63 - 94] years	[3 - 101 - 304] years	[0.13 - 0.23 - 0.36]
Epoch III	[80 - 106 - 142] years	[11 - 96 - 196] years	[0.30 - 0.42 - 0.50]

Mean values, 5th and 95th percentiles are reported, as a function of the sources of uncertainty considered.

Assuming the three epochs past record as independent samples and then maximizing the product of their likelihoods, we obtained **global results** consistent with the Epoch III activity except for a longer self-excitement.

	Renewal time $1/\lambda_0$	Self-excitement decay	Mean offspring
Global	**[82 - 105 - 140] years**	**[48 - 189 - 435] years**	**[0.26 - 0.41 - 0.59]**

A particular relevance was given to the estimates related to the most recent event in AD 1538, assuming that it started a new eruptive epoch.

The probability Q_{mn} of still having a Monte Nuovo offspring in the future is estimated as:
EI [0.0% - 3.8% - 10.1%] EII [0.0% - 0.0% - 0.2%] EIII [0.0% - 0.0% - 0.0%]

The likelihood L_{mn} of have observed 478 years without eruptions after Monte Nuovo event is:
EI [0.6% - 3.8% - 10.5%] EII [0.0% - 0.1% - 0.5%] EIII [0.2% - 0.9% - 2.3%]

	Q_{mn}	L_{mn}
Global	[0.0% - 0.3% - 1.6%]	[0.2% - 0.8% - 2.2%]

Several volcanological assumptions can modify the results.

1) Considering only the events occurred in **the first parts of the epochs** before the climatic eruptions, gives longer durations of the self-excitement decay, and slightly smaller base rates.

	Q_{mn}	L_{mn}
First parts	[0.0% - 7.6% - 18.0%]	[0.6% - 2.8% - 7.2%]

2) Separating the **western record** from the rest, the self-excitement behavior is weakened and the base rate drops down.

This increases the likelihood of having observed 478 years without activity after Monte Nuovo eruption.

	Q_{mn}	L_{mn}
Western	[0.0% - 0.0% - 0.0%]	[22.6% - 32.8% - 45.5%]

3) Fitting the model on the **whole eruptive record** including even the periods of quiescence produces lower base rates and longer duration of the self-excitement decay.

Anyways the **non-homogeneity** between the eruptive epochs and the periods of quiescence seems too strong to be captured without losing accuracy on the reproduction of the pattern inside epochs.

This assumption seemed better fitting on the western record separated, in this case producing base rates of one on ~1 ka, more compatible with the length of the **periods of quiescence**.

A probability density function for the **remaining time** before the next eruption at Campi Flegrei has been calculated.

We assumed a process Z_{mn} starting without excitement except for the residual additional intensity from Monte Nuovo event.

Again the different volcanological assumptions can change the results.

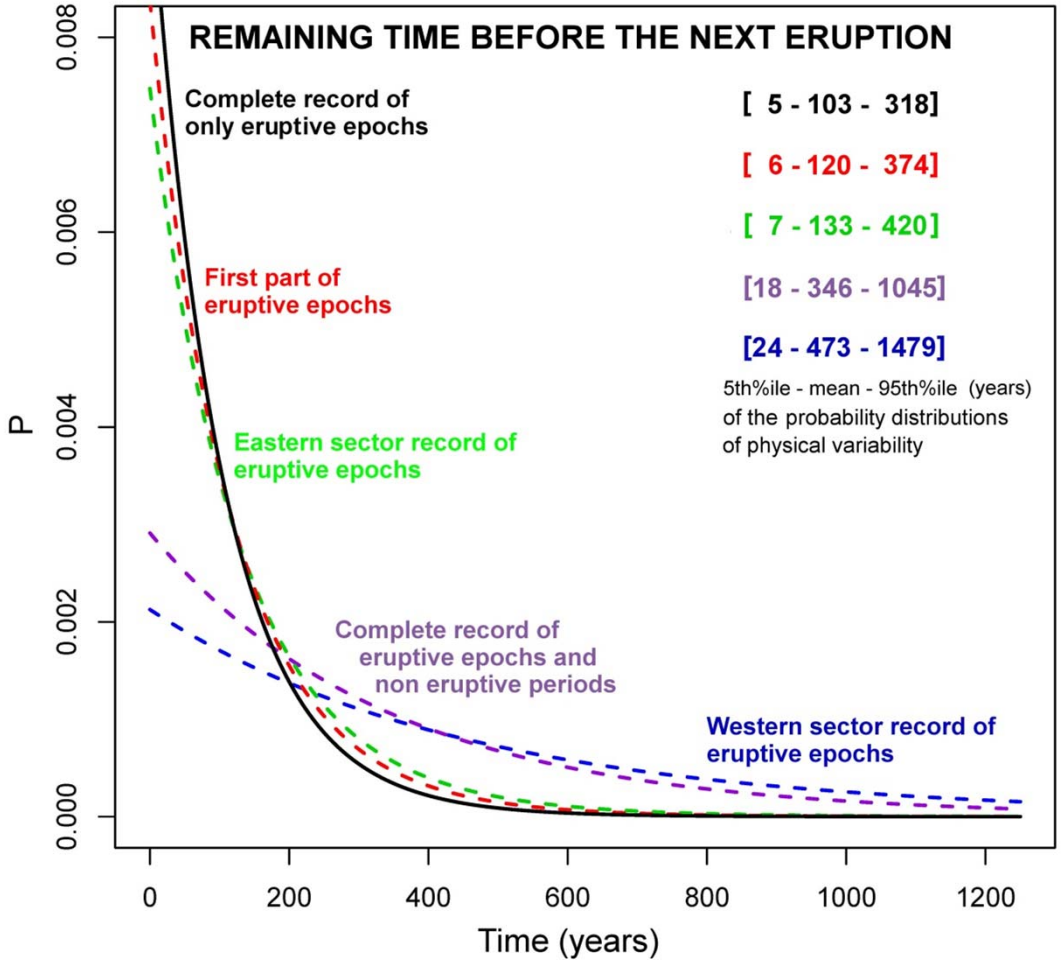

Fig 27. Mean probability density functions for the remaining time before the next eruption, assuming maximum likelihood exponential distributions.

Different colours correspond to alternative geological assumptions.

The values reported are the mean with respect to epistemic uncertainty of the 5^{th} and 95^{th} percentiles and the mean value of the physical variability

The mean and **uncertainty percentiles** of each probability density values can be reported, as a function of the considered epistemic uncertainty affecting the stratigraphic record.

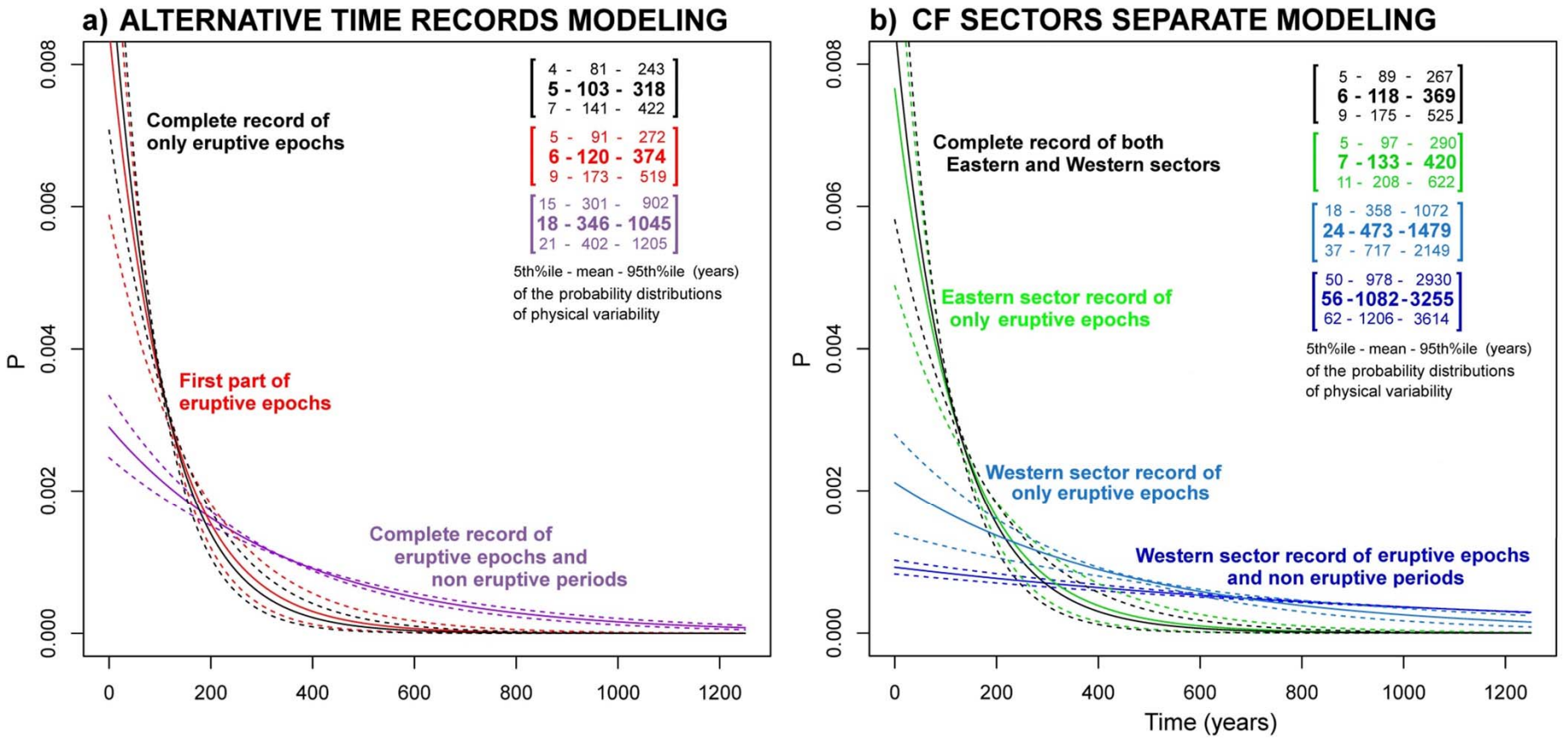

Fig 28. The bold lines indicate the mean probability density functions per year, and the dashed lines are composed of the 5*th* and 95*th* *e*pistemic uncertainty percentiles of the values of such functions.

The values reported are the 5*th* percentile, the mean and the 95*th* percentile with respect to epistemic uncertainty (from above to below), of the 5*th* percentile, the mean value and the 95*th* percentile of the physical variability (from left to right).

Concluding remarks

- **Doubly stochastic models** are a very general tool for assessing random systems that depend on uncertain information, as in the case of volcanic processes.

- The hazard assessment procedure applied at Campi Flegrei includes the quantification of some of the main sources of epistemic uncertainty by using performance-based **expert judgment techniques**.

- The '**logic tree**' approach is an easy method for combining alternative vent opening maps based on key volcanologic features, inside a doubly stochastic model.

- The PDC invasion area estimation based on **continuous probability** density functions extends the classical hazard approach relying on separate scenarios for specific eruption sizes.

- **Cox and Hawkes processes** allow to consider data uncertainty and to reproduce spatial and temporal clustering of eruptive events. In the study developed both these features were considered together for the first time.

Publications

Quantifying volcanic hazard at Campi Flegrei caldera (Italy) with uncertainty assessment: I. Vent opening maps, *A. Bevilacqua , R. Isaia, A. Neri, S. Vitale , W. P. Aspinall, M. Bisson, F. Flandoli, P. J. Baxter, A. Bertagnini, T. Esposti Ongaro, E. Iannuzzi, S. Orsucci, M. Pistolesi, M. Rosi,* J Geophys Res, 120 (4), 2309-2329.

Quantifying volcanic hazard at Campi Flegrei caldera (Italy) with uncertainty assessment: II. Pyroclastic density current invasion maps, *A. Neri, A. Bevilacqua, T. Esposti Ongaro, R. Isaia, W. P. Aspinall, M. Bisson, F. Flandoli, P. J. Baxter, A. Bertagnini, E. Iannuzzi, S. Orsucci, M. Pistolesi, M. Rosi, S. Vitale*, J Geophys Res, 120 (4), 2330-2349.

Temporal models with uncertainty assessments for the volcanism at Campi Flegrei (Italy), (in preparation).

Acknowlegments

This study was developed during the PhD scholarship at Istituto Nazionale di Geofisica e Vulcanologia and Scuola Normale Superiore di Pisa (Convenzione INGV-SNS 2009-2011).

The obtained results were made achievable thanks to the precious collaboration with many colleagues in the ambience of several research projects, including:

- **Project MED-SUV** "*Mediterranean Supersite Volcanoes*", European Union, 2013-2016.
- **Project DPC-V1** "*Valutazione della pericolosità vulcanica in termini probabilistici*", Dipartimento della Protezione Civile (Italy), 2012-2015.
- **Project EJN** "*Expert Judgment Network*", COST Action, European Union, 2013-2017.

SCUOLA NORMALE SUPERIORE

INGV

SEVENTH FRAMEWORK PROGRAMME

MEDiterranean SUpersite Volcanoes MED-SUV

PROTEZIONE CIVILE NAZIONALE

Unione Europea

cost EUROPEAN COOPERATION IN SCIENCE AND TECHNOLOGY